

Contents lists available at ScienceDirect

Petroleum Science

journal homepage: www.keaipublishing.com/en/journals/petroleum-science



Review Paper

Applications of molecular dynamics simulation in studying shale oil reservoirs at the nanoscale: Advances, challenges and perspectives



Lu Wang ^a, Yi-Fan Zhang ^{a, *}, Run Zou ^a, Yi-Fan Yuan ^a, Rui Zou ^a, Liang Huang ^a, Yi-Sheng Liu ^a, Jing-Chen Ding ^{a, c}, Zhan Meng ^{b, **}

- a State Key Laboratory of Oil and Gas Reservoir Geology and Exploitation, Chengdu University of Technology, Chengdu, 610059, Sichuan, China
- ^b School of Petroleum and Natural Gas Engineering, Southwest Petroleum University, Chengdu, 610500, Sichuan, China
- ^c Exploration and Development Research Institute, SINOPEC North China Company, Zhengzhou, 450006, Henan, China

ARTICLE INFO

Article history: Received 3 June 2024 Received in revised form 25 September 2024 Accepted 26 September 2024 Available online 27 September 2024

Edited by Yan-Hua Sun

Keywords:
Molecular dynamics
Shale oil reservoirs
Nanopores
Enhanced oil recovery
Fluid flow behavior
Shale oil occurrence

ABSTRACT

The global energy demand is increasing rapidly, and it is imperative to develop shale hydrocarbon resources vigorously. The prerequisite for enhancing the exploitation efficiency of shale reservoirs is the systematic elucidation of the occurrence characteristics, flow behavior, and enhanced oil recovery (EOR) mechanisms of shale oil within commonly developed nanopores. Molecular dynamics (MD) technique can simulate the occurrence, flow, and extraction processes of shale oil at the nanoscale, and then quantitatively characterize various fluid properties, flow characteristics, and action mechanisms under different reservoir conditions by calculating and analyzing a series of MD parameters. However, the existing review on the application of MD simulation in shale oil reservoirs is not systematic enough and lacks a summary of technical challenges and solutions. Therefore, recent MD studies on shale oil reservoirs were summarized and analyzed. Firstly, the applicability of force fields and ensembles of MD in shale reservoirs with different reservoir conditions and fluid properties was discussed. Subsequently, the calculation methods and application examples of MD parameters characterizing various properties of fluids at the microscale were summarized. Then, the application of MD simulation in the study of shale oil occurrence characteristics, flow behavior, and EOR mechanisms was reviewed, along with the elucidation of corresponding micro-mechanisms. Moreover, influencing factors of pore structure, wall properties, reservoir conditions, fluid components, injection/production parameters, formation water, and inorganic salt ions were analyzed, and some new conclusions were obtained. Finally, the main challenges associated with the application of MD simulations to shale oil reservoirs were discussed, and reasonable prospects for future MD research directions were proposed. The purpose of this review is to provide theoretical basis and methodological support for applying MD simulation to study shale oil reservoirs.

© 2024 The Authors. Publishing services by Elsevier B.V. on behalf of KeAi Communications Co. Ltd. This is an open access article under the CC BY-NC-ND license (http://creativecommons.org/licenses/by-nc-nd/4.0/).

1. Introduction

Currently, the development of conventional hydrocarbon reservoirs is insufficient to meet the growing global energy demand (Wang et al., 2023a). The global oil demand in 2023 set a new record, reaching 1388.56 \times 10^4 t/d (IEA, 2023). Vigorously developing unconventional hydrocarbon resources is imperative. The global

E-mail addresses: zyf_1839@163.com (Y.-F. Zhang), zhan.meng@swpu.edu.cn (Z. Meng).

shale oil resources are abundant, with an estimated recoverable reserve of 1501.3×10^8 t (Pang et al., 2023). The shale oil and gas revolution in the United States has changed the world energy landscape and promoted theoretical and technological progress in the development of shale oil and gas reservoirs (Li et al., 2022a). Statistics from the Energy Information Administration show that the remaining shale oil reserves in the United States are 325×10^8 t, with a total technically recoverable reserve of 262×10^8 t (U.S. Energy Information Administration, 2022). In comparison, China's total shale oil resources and technically recoverable reserves are only about 1/2 of those in the United States (Hu et al., 2020; Jiao et al., 2020). Additionally, countries such as Russia, Argentina,

^{*} Corresponding author.

^{**} Corresponding author.

Nomenclature		n(z)	Atomic number density, cm ⁻³		
		$P_{ii}(i = x,y,z)$ Pressure components in different directions, MPa			
\boldsymbol{a}_i	Acceleration of atom i, m/s ²	$P_{\alpha\beta}$	The pressure tensor of element $\alpha\beta$, MPa		
Α	Cross-sectional area of the nanopore, cm ²	\boldsymbol{r}_i	Position of the atom <i>i</i>		
D	Diffusion coefficient, cm ² /s	\mathbf{r}_{i}^{0}	Initial position of the atom <i>i</i>		
d	Dimensionality	$r_i(t_0)$	Position of the atom i at time t_0		
$\mathrm{d}P/\mathrm{d}z$	Displacement pressure gradient, MPa/m	T	System temperature, K		
dv/dr	Velocity gradient on the fictitious slip boundary, m/s	U	Total potential energy that depends on the		
E_1	Energy of material 1, kJ/mol		coordinates of the atoms in the system, kJ/mol		
E_2	Energy of material 2, kJ/mol	V	System volume, cm ³		
$E_{\rm interaction}$	Interaction energy between material 1 and material	$v_{\rm boundary}(z)$	z) Velocity of the fluid in the boundary layer, m/s		
	2, kJ/mol	$v_{\rm bulk}(z)$	Velocity of the fluid in the bulk phase, m/s		
$E_{ m total}$	Total energy of material 1 and material 2, kJ/mol	\boldsymbol{v}_i	Velocity of the atom i , m/s		
f	External force, N	\mathbf{v}_i^0	Initial velocity of the atom i , m/s		
\boldsymbol{F}_i	The force of atom <i>i</i> , N	$v_{ m surf}$	Slip velocity on the fictitious slip boundary, m/s		
J_{M}	The ending time step of the parameter averaging	$ u_{t}$	Total velocity, m/s		
J_{N}	The starting time step of the parameter averaging	v(t)	Velocity of the atom i at time t , m/s		
$k_{ m B}$	Boltzmann constant	w	Width of bulk phase, nm		
L	Thickness of the region $\{a,b\}$, nm	$w_{ m boundary}$	Thickness of the boundary layer, nm		
L_{s}	Slip distance on the fictitious slip boundary, nm	Z_{IJ}	Coordinate of the midpoint of the <i>n</i> -th bin		
L_{z}	Simulation box size perpendicular to the interface	z_{lower}	The lower boundary of each region		
	along the z direction, nm	$Z_{\rm upper}$	The upper boundary of each region		
l_z	Length of any segment containing the interface along	α	A constant related to the density distribution		
	the z direction, nm	heta	Angle between head-to-tail vector of the molecule		
	Fitting constants		and the z axis		
$M_{ m i}$	Molecular weight, g/mol	η	Fluid viscosity, mPa·s		
m_i	Mass of atom i, g	$\eta_{ m bulk}$	Viscosity of the fluid in the bulk phase, mPa s		
N	Total number of time steps averaged over	$ ho_{ ext{mas}s}$	Macroscopic density, g/cm ³		
N_{A}	Avogadro constant	ρ_{number}	Number density, cm ⁻³		
` /	Number of molecules in the range of radius r to $r+\Delta r$	() () ()	Average value		
$N(t_0)$	Total number of particles in the specified region at t	$\langle \Delta x^2(t) \rangle_{\{a\}}$	MSD of particles that remain in region $\{a,b\}$ in the x		
NT/	moment		direction		
$N(t_0, t_0 +$	t) Number of particles in the specified region from t_0				
	moment to $t_0 + t$ moment				

Australia, and Mexico also have abundant shale oil resources (Li et al., 2022b). Therefore, effective development of shale oil reservoirs can alleviate the current global energy shortage.

At present, numerous reports have addressed the reservoir characteristics, fluid properties, and enhanced oil recovery (EOR) in shale oil reservoirs (Xu et al., 2022a). Regarding reservoir characteristics, micro- and nano-pores and micro-fractures provide the main storage space for shale oil. Zhou et al. (2020) investigated the pore structures and spatial distribution patterns of shale reservoirs by core analysis, scanning electron microscopy (SEM), confocal laser scanning microscopy (CLSM), and nuclear magnetic resonance (NMR). Donadelli et al. (2019) revealed the type and maturity of kerogen in shale samples using X-ray photoelectron spectroscopy (XPS). Shale reservoirs not only have complex pore throat structures but also have diverse occurrence states of shale oil (Gant and Anderson, 1988; Dubey and Waxman, 1991; Li et al., 2020a). Chen and Zhang (2017) obtained free oil and adsorbed oil through continuous extraction of oil-bearing shale samples using different solvents. Li et al. (2020b) characterized the content of free oil and adsorbed oil in cores using the Rock-Eval pyrolysis method. It should be noted that the low petrophysical properties, strong heterogeneity, and high clay mineral content result in extremely low oil recovery through depletion exploitation (Wang et al., 2023a). Therefore, scholars have also conducted a series of investigations to enhance shale oil recovery (Sheng, 2015; Sambo et al., 2023). Du et al. (2023) combined computed tomography (CT) and NMR tests to study the EOR mechanism of air injection in

shale oil reservoirs. Zhang et al. (2018a) studied the effects of matrix permeability, gas injection parameters, and stress variations on CO₂ injection to enhance oil recovery (CO₂-EOR) by numerical simulation. In addition, many on-site tests of CO₂ injection into shale reservoirs have been conducted around the world. However, gas channeling, low miscibility, or other unknown reasons have led to unsatisfactory improvements in oil recovery (Jacobs, 2016). Therefore, revealing the fluid behavior and EOR mechanism of shale oil at the micro-scale is the prerequisite. Molecular dynamics (MD) is already an effective method for studying shale reservoirs at the microscale (Sun et al., 2023a). The fluid distribution characteristics (Wang et al., 2023b), molecular transfer behavior (Wang et al., 2023c), and micro-mechanism of EOR (Yuan et al., 2023) can be revealed by MD.

Some specific aspects of MD investigations in shale reservoirs have been summarized in several reviews. Wang et al. (2021) provided a comprehensive review of the shale gas adsorption characteristics in inorganic, organic, and inorganic-organic composite nanopores. Lan et al. (2019) and Wang et al. (2019) focused on the desorption processes and seepage mechanisms of shale gas. Compared with shale gas, shale oil contains complex components such as heavy hydrocarbons, aromatic hydrocarbons, and non-hydrocarbon compounds, which makes the interaction between shale oil and mineral walls intricate. Therefore, predicting the fluid behavior and recovery process of shale oil is more challenging. Considering these factors, Zhang et al. (2022) reviewed the molecular simulation studies of kerogen's structure, geological

processes, interactions with minerals, and pyrolysis. Sun et al. (2023a) mainly introduced the studies of MD simulation in the adsorption, diffusion and flow of shale oil and gas. Huang et al. (2024) summarizes recent advances in molecular dynamics simulations for shale oil flow as well as enhanced recovery. Liu et al. (2024) reviewed microscopic mechanisms of enhancing shale oil recovery through CO2 flooding. However, there are a limited number of review articles on MD, especially for shale oil reservoirs. Jia et al. (2019) reviewed the impact of nanopore confinement effect on fluid phase behavior and oil recovery. Dong et al. (2022a) reviewed the CO2-kerogen interaction and its impact on CO2-EOR. However, previous reviews have primarily focused on specific aspects of reservoir characteristics, fluid behavior, or recovery methods. More importantly, the previous reviews did not discuss the challenges of MD methods in shale oil reservoirs, and the summary of research prospects was not specific and sufficient. Therefore, it is necessary to systematically review the application of MD simulation in the occurrence characteristics, flow behavior, and EOR methods of shale oil, and consider the interconnections and interactions among these three aspects. Furthermore, challenges related to the scale, realism, and application of MD simulations should be thoroughly summarized, and prospects of detailed solutions should be proposed.

The principle of MD was first introduced, and the applicability of force fields and ensembles in shale reservoirs was also summarized. Subsequently, the calculation methods for MD parameters reflecting fluid properties were given. Then, various applications of MD simulation in studying the occurrence characteristics, flow behavior, and EOR of shale oil were summarized. The effects of pore size and structure, wall types and roughness, reservoir temperature and pressure, fluid injection and production parameters, oil component, formation water, and inorganic salt ions were also analyzed. Finally, the main challenges encountered by MD simulation of shale oil reservoirs at this stage were discussed, and reasonable prospects for future research directions were proposed.

2. Molecular dynamics methods

Both the development of nanopores and the complex properties of rocks and fluids in shale oil reservoirs result in difficulties in simulating the occurrence, flow, and recovery processes of shale oil at the nanoscale by physical simulation experiments and reservoir numerical simulations. By contrast, MD analyzes the coordinates and velocity information of atoms in the system using statistical mechanics methods, thereby obtaining a series of macroscopic properties of the system. MD is mainly used for simulating multicomponent fluid behavior (Frenkel and Smit. 2002). Therefore, the MD method is suitable for studying multiphase fluid interactions and micro mechanisms in shale reservoirs. The common process for MD research on shale oil reservoirs is shown in Fig. 1. Firstly, it is necessary to simplify the actual shale reservoir conditions to make MD simulation implementable. Subsequently, the pore model and oil system need to be constructed and combined. On this basis, a series of EOR measures such as gas-injection flooding and gas-injection huff-n-puff may be implemented. Then, the model after energy minimization is subjected to dynamic simulation. Finally, the fluid behavior and EOR mechanism can be revealed by calculating and analyzing various microscopic parameters. Therefore, the MD principle was first introduced in this section. Then, the selection of force fields and the application of ensembles, which are crucial for MD simulation, were summarized. Additionally, the calculation methods for frequently used MD parameters were listed.

2.1. Molecular dynamics principles

Compared with quantum mechanics (QM) based on the Schrödinger equation, molecular mechanics (MM) is a simplified method that describes the interactions between particles through parameterized force fields (Mao et al., 2023). Classical Newtonian mechanics based on MM can be used to describe the forces on particles with velocities far less than the speed of light (Eq. (1)) (Marx and Hutter, 2009). Classical MD calculates the acceleration of each atom according to Newton's second law (Eq. (2)), and then integrates the motion equation over time to obtain the motion trajectory of particles in the system (Eqs. (3)–(5)), thereby further calculating the thermodynamic quantities and other macroscopic properties of the system (Haile et al., 1993). Although classical MD ignores the motion of electrons inside atoms to achieve simulations at relatively long-time scales and big spatial scales, it can still achieve accuracy comparable to QM to a certain extent (Van Gunsteren and Berendsen, 1990; Hockney and Eastwood, 2021).

$$\mathbf{F}_{i} = -\nabla_{i}U = -\left(\mathbf{i}\frac{\partial}{\partial x_{i}} + \mathbf{j}\frac{\partial}{\partial y_{i}} + \mathbf{k}\frac{\partial}{\partial z_{i}}\right)U \tag{1}$$

$$\boldsymbol{a}_i = \frac{\boldsymbol{F}_i}{m_i} \tag{2}$$

$$\frac{\mathrm{d}^2}{\mathrm{d}t^2} \mathbf{r}_i = \frac{\mathrm{d}}{\mathrm{d}t} \mathbf{v}_i = \mathbf{a}_i \tag{3}$$

$$\mathbf{v}_i = \mathbf{v}_i^0 + \mathbf{a}_i t \tag{4}$$

$$\mathbf{r}_i = \mathbf{r}_i^0 + \mathbf{v}_i^0 t + \frac{1}{2} \mathbf{a}_i t^2 \tag{5}$$

2.2. Force fields

The core of MD simulation is the force field, an empirical potential function that describes the interactions between atoms. The fitting parameters in the function usually come from neutron diffraction, X-ray diffraction, electron diffraction, infrared spectroscopy, Raman spectroscopy, and QM calculations (McArdle et al., 2020). This is the significant reason why classical MD can achieve high accuracy while ignoring electron motion.

Quartz (Wang et al., 2023c), calcite (Dong et al., 2023a), illite (Dai et al., 2023), kaolinite (Wang et al., 2023b), and montmorillonite (Huang et al., 2021) are commonly used in MD simulation to characterize the inorganic wall of shale, while kerogen or graphene is used to characterize the organic wall (Dong et al., 2022a). Additionally, MD research on shale oil reservoirs also involves the simulation of various fluids, including CO₂, H₂O, hydrocarbons, and other compounds (Dai et al., 2023; Wang et al., 2023c). Only by selecting appropriate force fields for different materials can reasonable results be obtained.

Commonly used force fields and their applicability were summarized in Table 1. Generally, quartz and calcite can be parameterized using the COMPASS force field (Xue et al., 2015), and there are also studies using CLAYFF to parameterize quartz (Dash and Rath, 2020; Xu et al., 2022b). UFF (a universal force field superior to DREIDING) and CLAYFF are commonly used for kaolinite. PCFF, COMPASS, CVFF, and OPLS are usually used to parameterize organic matter (Sun et al., 2023a). It is reported that COMPASS outperforms UFF, DREIDING, PCFF, and CVFF in predicting the density of hexane (Moradi et al., 2023). The original OPLS-AA (all-atom) force field

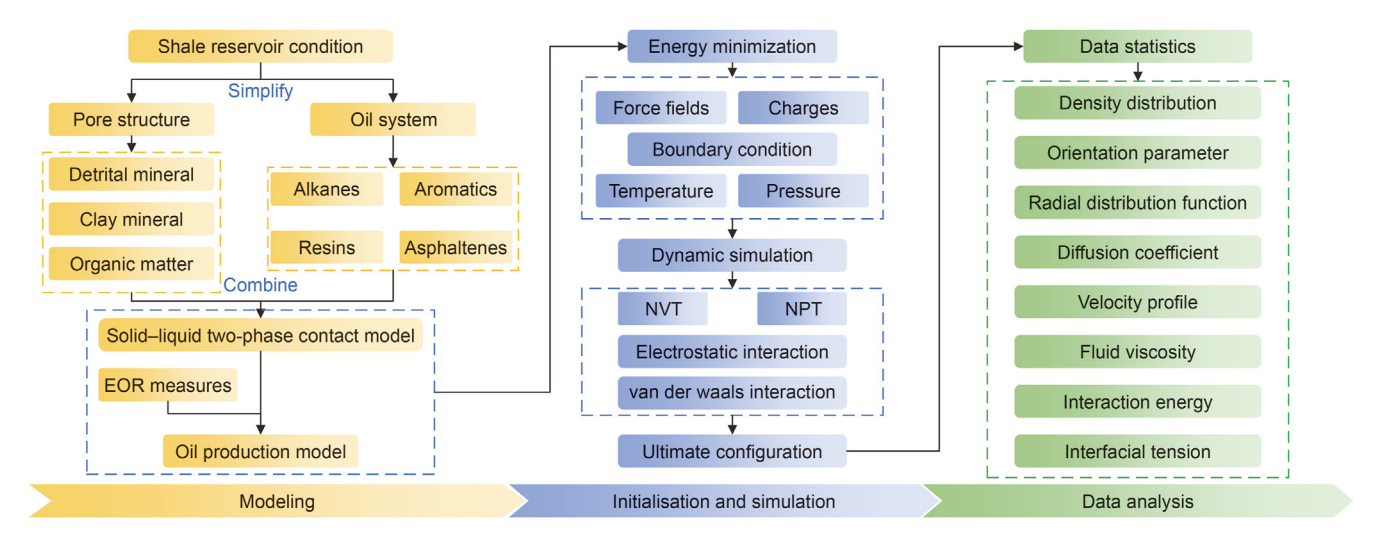


Fig. 1. Flow chart for MD simulation of shale oil reservoirs.

Table 1Commonly used force fields and their applicability.

References	Force fields	Advantages/limitations	Applicability	Examples in shale oil reservoirs
Sun (1995)	PCFF (polymer consistent force field)	High accuracy and consistency/complex potential functions and computationally demanding	Polymers, organic materials, and approximately 20 inorganic metals	Parameterization of kerogen in the optimization of kerogen molecular structure (Sun et al., 2020)
Sun et al. (1998)	COMPASS (condensed- phase optimized molecular potentials for atomistic simulation studies)	High accuracy in predicting various properties of molecules in condensed phases/complex potential functions	Various large and small molecules, including organic molecules, gaseous molecules, and inorganic molecules	Parameterization of oil molecules in the investigation of occurrence characteristics of shale oil (Tian et al., 2017)
Dauber-Osguthorpe et al. (1988)	CVFF (consistent-valence force field)	High precision and consistency/inability to describe inorganic systems	Small organic crystals, gas phase structures, peptides, proteins, and various organic systems	Parameterization of octane in the investigation of multi- component interactions (Ho and Wang, 2019)
Mayo et al. (1990)	DREIDING	Simplified parameters and computationally efficient/limited in predicting charge distribution within the molecule and van der Waals interactions	Predicting structures and dynamics of organic, biological, and main-group inorganic molecules	Parameterization of methane in the investigation of methane adsorption in nanopores (Zhang et al., 2018b)
Vanommeslaeghe and MacKerell Jr (2012) and Vanommeslaeghe et al. (2012)	CGenFF (CHARMM General Force Field)	Simple potential functions and flexible/limited in describing hydrogen bonds	Organic small molecules, polymers, biological molecules, etc.	Parameterization of oil in the clay nanopores with brine (Zhang et al., 2019a)
Jorgensen et al. (1996)	OPLS (optimized potentials for liquid simulations)	High accuracy and applicability to various solid, liquid, and gas phases substances/inability to describe extremely complex systems (e.g. metal-organic frameworks)	Proteins, nucleic acids, organic molecules, etc.	Parameterization of decane in the investigation of flow characteristics of decane (Zhang et al., 2016)
Cygan et al. (2004)	CLAYFF (clay force field)	Computationally efficient and high accuracy in describing clay minerals/limited application scope	Montmorillonite, illite, water, etc.	Parameterization of montmorillonite and illite during the nanopores construction (Zhang, et al., 2016, 2019a)

tends to overestimate the viscosity of hydrocarbons. Allen and Rowley (1997) regressed a relatively small value of $\sigma_{\rm H}$ (hydrogen LJ σ) used in conjunction with the OPLS-AA model. With this value of $\sigma_{\rm H}$, the OPLS-AA model is capable of reasonably accurate viscosity predictions, and values within 10%–20% of the experimental can reasonably be expected. By contrast, united-atom force fields consistently under-predict the viscosity of long-chain linear alkanes, with the prediction accuracy deteriorating when longer-chain molecules or high pressures are used (Payal et al., 2012). Notably, united-atom force fields significantly reduce the number of atoms for which non-bonded interactions need to be calculated, thereby greatly improving computational efficiency. In addition, there are many force field models suitable for small molecules. For example, TraPPE describes methane molecules (Martin and

Siepmann, 1998), EPM2 and TraPPE describe CO₂ molecules (Harris and Yung, 1995), and SPC, SPC/E, TIP3P, and TIP4P describe H₂O molecules. TraPPE is a better choice for the transport characteristics of pure CO₂. EPM2 is improved based on the EPM, and the improvements make only a slightly higher critical value compared to the experimental value. Furthermore, both SPC and TIP3P force fields have low computational costs, making them suitable for simulations of large-scale systems. SPC/E is an improved version of the SPC model that includes partial corrections for polarization effects. Therefore, it performs better in describing the physical properties of water, such as density, diffusion coefficient, and dielectric constant. TIP4P adds a virtual point based on TIP3P to better simulate the dipole moment of water molecules, which is more suitable for the study of phase transition of water,

solute—solvent interaction in solution and interface phenomena (Jorgensen et al., 1983; Berendsen et al., 1987). These models optimize the molecular structure, potential energy function, and force field parameters of small molecules, which ensures simulation accuracy while also improving efficiency. Moreover, the CGenFF is a suitable choice for oil molecules in clay nanopores if the research object includes brine. In this case, water should be parameterized by TIP3P.

2.3. Ensemble

An ensemble refers to a large collection of systems that share the same properties and structural characteristics but are independent of each other. Commonly used ensembles include the microcanonical ensemble (NVE), grand canonical ensemble (μVT), canonical ensemble (NVT), and isothermal-isobaric ensemble (NPT) (Rapaport, 2004). A system using the NVE ensemble is isolated, with no energy exchange with its surroundings. This ensemble is usually applied to the piston plate used to push the fluid during the non-equilibrium dynamics simulation to reduce the interference of the piston plate on the thermal motion of fluid molecules. In the μVT ensemble, the number of particles in the system is not fixed (Haile, 1992). It is commonly used in the study of gas adsorption, especially irregular nanopores such as kerogen matrix nanopores. Therefore, the commonly used ensembles in MD studies of shale reservoirs are NVT and NPT. NVT can equilibrate the system temperature and is mainly used for dynamic relaxation to calculate the trajectory of fluid molecules in shale nanopores (Haile, 1992), NPT can equilibrate the temperature and pressure of the system and is mainly used in the simulation of condensed phase properties to equilibrate fluid density and pressure in shale nanopores (Andersen, 1980). Although the NPT ensemble simultaneously controls both temperature and pressure, volume adjustment introduces additional degrees of freedom, leading to complex coupling between temperature and pressure. Therefore, the temperature can be further equilibrated, and the MD results can be output from the NVT ensemble after pressure stability is achieved in the NPT ensemble.

2.4. Molecular dynamics parameters

Applying physical simulation can obtain density, viscosity, and PVT of shale oil, as well as minimum miscible pressure (MMP) and recovery factor (RF) during gas injection. However, limitations in experimental conditions and spatial scale lead to differences between experimental results and actual conditions. By contrast, MD simulation can quantitatively characterize various fluid properties, flow characteristics, and action mechanisms under high temperature and pressure simulation conditions by calculating microscale MD parameters (Wang et al., 2023a). The calculation expressions and applicability of commonly used MD parameters in investigations of shale oil reservoirs are summarized in Table 2. These MD parameters can be used to quantitatively characterize fluid properties and fluid—wall interactions at the nanoscale.

3. Occurrence characteristics of shale oil in nanopores

3.1. Occurrence characteristics of shale oil in different mineral types of nanopores

The prerequisite for revealing the flow behavior and EOR mechanism of shale oil is to clarify the occurrence characteristics of shale oil in nanopores (Zhu et al., 2019). Previous studies have confirmed that the mineral composition of reservoirs directly affects pore morphology, size, wettability, and other properties,

thereby affecting the occurrence characteristics of shale oil (Mohammed and Mansoori, 2018; Gong et al., 2024). Molecular dynamics studies of the occurrence characteristics of shale oil in different mineral types of nanopores are summarized in Table 3. Some studies have shown that shale oil exhibits multi-layer adsorption in nanopores, and the density of the adsorption layer decreases from the rock wall to the middle of the nanopores. The increase in ambient temperature increases the kinetic energy of molecules, resulting in a decrease in the density of the adsorption layer (Tian et al., 2018). By contrast, the increase in pressure may cause a slight increase in the density of the oil adsorption layer (Sponer et al., 1999). But in general, the occurrence characteristics of hydrocarbons in nanopores are insensitive to pressure (Sui et al., 2020; Cao et al., 2021). In addition, the adsorption capacity of oil molecules on the rock wall increases as the nanopore size decreases, resulting in a decrease in the number of oil adsorption layers. Additionally, the volume of free oil in the middle of the nanopores also continues to decrease (Fig. 2(a)) (Wang et al., 2015, 2016a). It is worth noting that the adsorbed octane molecules tend to be distributed parallel to the wall, whereas free molecules far away from the rock wall are randomly distributed in the nanopores, and the diffusion ability of adsorbed molecules is weaker than that of free molecules (Fig. 2(b)) (Wang et al., 2016b). Furthermore, dodecane molecules near the calcite wall are more neatly arranged (Fig. 2(c)) (Badwaik et al., 2023). This means that the closer the oil molecules are to the wall, the stronger the adsorption.

Some scholars have developed composite mineral nanopores to make the MD model closer to the actual nanopores. The occurrence state of shale oil in illite-kerogen nanopores indicates that a portion of oil molecules are adsorbed on the surface of illite and kerogen, but a considerable amount of oil molecules is dissolved in kerogen (Fig. 2(d)) (Kim and Devegowda, 2022). Moreover, the variation in wettability at both ends of kaolinite—kerogen composite pores significantly influences the occurrence characteristics of shale oil. It can be seen from Fig. 2(e) that water molecules form a water film when adsorbed on gibbsite, whereas oil molecules can form a dense oil film when adsorbed on siloxane and kerogen (Yang et al., 2023). This is because the gibbsite surface of kaolinite is hydrophilic, whereas the siloxane surface of kaolinite and kerogen are lipophilic.

3.2. Occurrence characteristics of shale oil with different components in nanopores

The composition of shale oil is complex, mainly including alkanes, aromatics, resins, and asphaltenes (Song et al., 2020). Different components in shale oil can interact with each other and affect their respective occurrence states. Compared with methane and propane, octane exhibits stronger dispersion forces with the walls (dispersion forces correlate positively with molecular weight) (Mavroyannis and Stephen, 1962). This results in the adsorption layer near the wall predominantly composed of octane, while light components primarily remain free in the nanopores (Dong et al., 2022b). Consequently, it can be inferred that the presence of appropriate amounts of heavy components within nanopores promotes the diffusion and migration of light components. Asphaltene is also more easily adsorbed on the kerogen wall than methane and *n*-octane (Wang et al., 2022a). These results indicate that heavy components are preferentially adsorbed on walls (Herdes et al., 2018). Furthermore, the polarity of aromatic cores in asphaltene and the polar groups that can form hydrogen bonds with Si-OH at the quartz surface both provide driving forces for adsorption (Xue et al., 2022). It is reflected that the affinity of various mineral components to various functional groups in oil molecules is different. Generally, non-polar components are

Table 2Calculation expressions and applicability of commonly used MD parameters.

References	Parameters	Expressions	Applicability
Li et al. (2010)	Density distribution	$\rho_{\rm mass} = \frac{10^{21}}{N_{\rm A}} M_i \rho_{\rm number} =$	Occurrence state of fluids in nanopores
		$\frac{1}{A\Delta z(J_{M} - J_{N} + 1)} \sum_{J=J_{N}}^{J_{M}} \sum_{l=1}^{N} H_{n}(z_{l,l})$	
Rigby and Roe (1988)	Orientation parameter	$S(z) = 1.5\langle \cos^2 \theta \rangle - 0.5$	Distribution state of fluid molecules relative to the wall
Kirkwood and Boggs (1942)	Radial distribution function (RDF)	$g(r) = \frac{N(r + \Delta r)}{4\pi \rho_{\text{number}} r^2 \Delta r}$	Affinity between different elements
Einstein (1905) and Von	, ,	Einstein–Smoluchowski relation:	Mobility of fluid molecules in nanopores
Smoluchowski (1906)		$D = \frac{1}{2d} \lim_{t \to \infty} \frac{1}{t} \langle [r_i(t_0 + t) - r_i(t_0)]^2 \rangle$	
Green (1952) and Kubo (1957)		The velocity auto-correlation function in a Green	
		-Kubo relation: $D = \frac{1}{d} \int_0^\infty dt \langle v_i(t) \cdot v_i(0) \rangle$	
Liu et al. (2004) and Mercier Franco et al. (2016)		$D_{XX}(\{a,b\}) = \lim_{t \to \infty} \frac{\langle \Delta x^2(t) \rangle_{\{a,b\}}}{2tP(t)}$	Mobility of fluid molecules confined in the z direction
		$D_{zz} = \frac{L^2}{\alpha \int_0^{+\infty} P'(t) dt}$	
Green (1952) and Kubo (1957)	Fluid viscosity	Green–Kubo relation: $\eta = \frac{V}{k_{\rm B}T} \int_0^\infty \langle P_{\alpha\beta}(t) \cdot P_{\alpha\beta}(0) \rangle dt$	Evaluation of fluid properties and flow behavior in nanopores (equilibrium molecular dynamics)
Zhan et al. (2020) and Botan et al. (2011)		$\eta = \frac{\int \int_{z_{\text{lower}}}^{z_{\text{upper}}} n(z) dz}{2a(z_{\text{upper}} - z_{\text{lower}})} \times \frac{1}{1.4386894 \times 10^{-5}}$	Viscosity of fluids in different regions (non-equilibrium molecular dynamics)
Liu et al. (2022a)	Velocity profile	$v_{\text{bulk}}(z) = -\frac{\text{d}P/\text{d}z}{2\eta_{\text{bulk}}} \left(z^2 - \frac{w^2}{4} - wL_s \right)$	Fluid velocity in the bulk region of nanopores
		$v_{\text{boundary}}(z) = \frac{v_{\text{slip}}}{w_{\text{boundary}}^2} \left(z - \frac{w}{2} - w_{\text{boundary}} \right)^2$	Fluid velocity in the boundary layer of nanopores
Šponer et al. (1999)	Interaction energy	$E_{\text{interaction}} = E_{\text{total}} - (E_1 + E_2)$	Quantitative evaluation of fluid—fluid and fluid—wall interactions
Van Buuren et al. (1993) and Makimura et al. (2013)	Interfacial tension (IFT)	$\gamma = \frac{1}{2} \left(p_{zz} - \frac{p_{xx} + p_{yy}}{2} \right) L_z$	Interfacial properties between different phases and calculation of minimum miscible pressure

Note: Only the core formulas are shown in Table 2, and the detailed derivations and definitions can be found in Supplementary Material.

Table 3MD studies of the occurrence characteristics of shale oil in different types of nanopores.

References	Mineral types	Force fields	Temperature, K	Pressure, MPa	Research results
Sui et al. (2020)	Dolomite	COMPASS	353	30	The number of free oil molecules decreases with the decrease of pore size.
Cao et al. (2021)	Montmorillonite, kaolinite, illite	UFF	358	30	The hydrocarbon adsorption capacity of montmorillonite is stronger than that of illite and kaolinite.
Dong et al. (2022b)	Quartz, graphene	OPLS-UA CHARMM	350	30	The density of adsorbed oil in graphene nanopores is higher than that in quartz nanopores.
Zeng et al. (2023)	Quartz	COMPASS	363	40	The adsorption capacity of methyl-modified quartz nanopore for oil is stronger than hydroxyl-modified quartz nanopore.
Huang et al. (2023)	Illite, quartz, calcite, albite, kerogen	COMPASS PCFF+	408.15	37.5	The adsorption effect of oil by rock minerals from strong to weak is kerogen, illite, albite, calcite, and quartz.
Badwaik et al. (2023)	Calcite, mica, silica	CLAYFF OPLS-UA potentials (Lee and Rossky, 1994)	300	_	The dispersion interaction between calcite and dodecane is the strongest.
Liang et al. (2022)	Quartz-illite	CLAYFF OPLS-AA	363-383	27.56 -37.69	The adsorption capacity of quartz-illite composite for oil is between that of quartz and illite.
Kim and Devegowda (2022)	Illite-kerogen	CLAYFF CVFF OPLS	355	30	A portion of oil can be dissolved in the kerogen.
Yang et al. (2023)	Gibbsite-kerogen and siloxane-kerogen	CLAYFF CVFF OPLS SPC/E	353	25	The presence of water can shield the influence of hydrophilic surfaces on the adsorption behavior of shale oil.

adsorbed by kerogen mainly through van der Waals interaction, whereas oil molecules containing polar functional groups have additional large Coulombic forces with kerogen, resulting in relatively strong adsorption (Fig. 3(a)) (Fei et al., 2023). More importantly, the Coulomb force appears to correlate negatively with molecular weight, implying that the occurrence state of small oil molecules is significantly affected by functional groups. Previous

studies have demonstrated that both quartz and kerogen exhibit strong adsorption of toluene, indole, and nonanone, and kerogen also shows a preference for methyl octyl sulfide in the presence of sulfur element (Sun et al., 2023c). It can be seen from Fig. 3(b) that highly polar groups containing hydrogen can form hydrogen bonds (H-bongs) with hydroxyl quartz walls (Wang et al., 2023b). Molecules containing nitrogen elements are attracted by oxygen

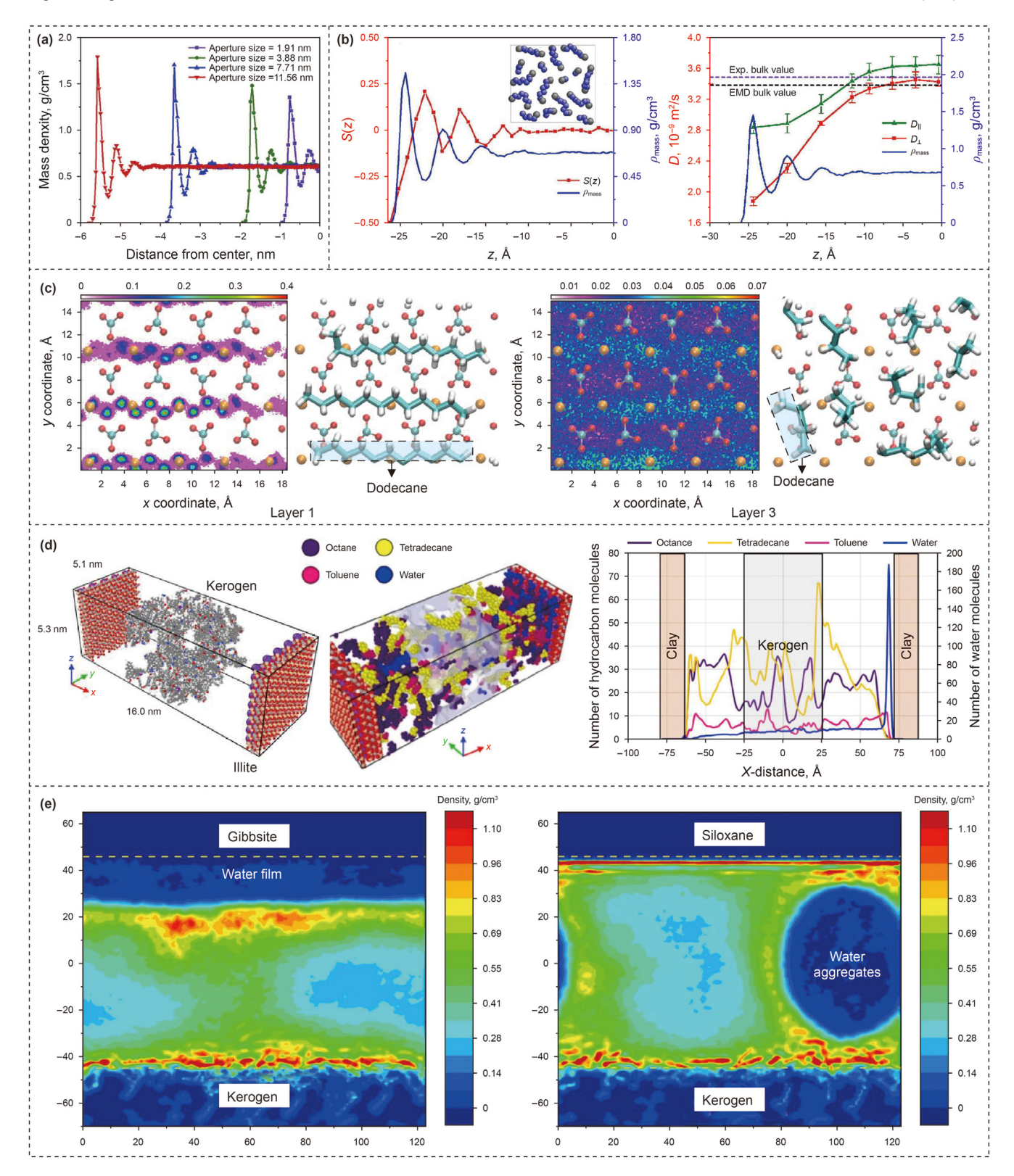


Fig. 2. Occurrence characteristics of shale oil in nanopores. (a) Density profiles of *n*-pentane in graphene nanopores with different sizes (Wang et al., 2015); (b) Density distribution, orientation parameter, and diffusion coefficient of *n*-octane in quartz nanopores (Wang et al., 2016b); (c) Two-dimensional density distribution and structure of dodecane in the first and third adsorption layers on calcite walls (Badwaik et al., 2023); (d) Illite–kerogen nanopore configuration, occurrence states of shale oil and water and density distribution of shale oil and water (Kim and Devegowda, 2022); (e) Two-dimensional density distribution of shale oil in the kaolinite (gibbsite)–kerogen nanopore and kaolinite (siloxane)–kerogen nanopore (Yang et al., 2023).

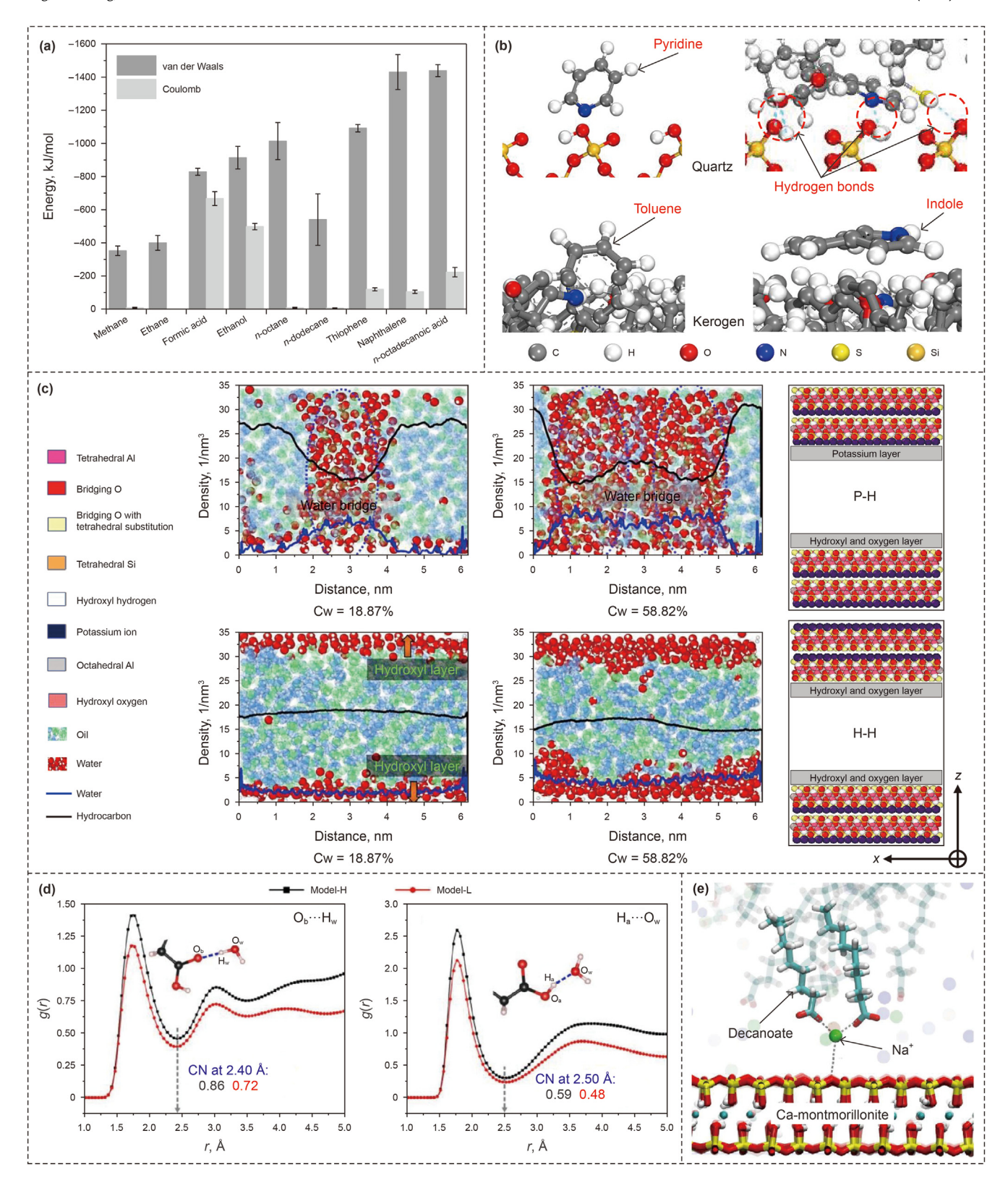


Fig. 3. Occurrence characteristics of different compounds. (**a**) Interaction energy between kerogen and different components (Fei et al., 2023); (**b**) Distribution diagrams of different oil molecules on the surfaces of quartz and kerogen; (**c**) Equilibrium configurations and number density profiles (*z*-direction) of water and oil (Xiong et al., 2020); (**d**) RDF of O_b (carbonyl oxygen)— H_w (hydrogen in water) and H_a (carbonyl hydrogen)— O_w (oxygen in water), model-H (model-H) with a high (low) content of brine (Zhang et al., 2019a); (**e**) Cation bridge between montmorillonite and decanoate (Underwood et al., 2015).

elements from rock walls (Zhang et al., 2023a). Molecules containing benzene rings are easily attracted by kerogen (Zhang et al., 2023a). These factors all lead to stronger adsorption of oil molecules by walls and weaker mobility of oil.

Formation water in shale reservoirs significantly impacts the occurrence state of shale oil in nanopores (Yu and Sheng, 2017; Li et al., 2020c). It is reported that the strong lipophilicity of kerogen makes water molecules present in the form of water clusters (water films) above the oil layer when the water content is low (high) (Wang et al., 2025). By contrast, the strong hydrophilicity of illite allows water molecules to form a water film and tightly adsorbed onto the wall surface. Additionally, the induced electric field in potassium-hydroxyl (P-H) illite nanopores can promote the formation of water bridges. The higher the water content, the wider the water bridge (Fig. 3(c)) (Xiong et al., 2020). However, the electric field strength is weakened by the charge screening effect of counter ions as the salinity increases, leading to a decrease of surface potentials in the interior region of the nanopore, thereby reducing the thickness of the water bridge until it completely disappears (Xiong et al., 2020; Xiong and Devegowda, 2022). In addition, brine tends to cover the surface of montmorillonite, preventing shale oil from contacting it. In this case, nonpolar components are evenly distributed in the nanopore, while organic acids can form H-bongs with water molecules (Fig. 3(d)), leading to a large amount of organic acid aggregation at the oil-brine interface (Zhang et al., 2019a). In addition, organic acids can be adsorbed on the clay surface through Na⁺ cation bridges (Fig. 3(e)) (Underwood et al., 2015). Notably, the cation bridging mechanism is prevalent in initially oil-wet clay, whereas it is absent in initially water-wet clay. Fig. 2(e) shows that the siloxane surface of kaolinite is lipophilic. Na⁺ and Ca²⁺ can be adsorbed on the siloxane surface and coordinated by water molecules as an outersphere complex, making the siloxane surface hydrophilic (Zhang et al., 2016). Brine can also alter the wettability of calcite (Cooke et al., 2010). Na⁺ and Cl⁻ can be adsorbed on negatively charged and positively charged calcite surfaces (different crystal surfaces of calcite), respectively. Moreover, both Na⁺ and Cl⁻ have strong hydration capacity, which makes calcite more hydrophilic (Zhao et al., 2019). Therefore, the adsorption effect of calcite on oil molecules is weakened. Nevertheless, there is still a lack of MD research on the effects of inorganic salt ion types and concentrations on the occurrence characteristics of shale oil in various of organic nanopores.

4. Flow behavior of shale oil in nanopores

4.1. Effects of nanopore type and reservoir conditions

The evaluation of the mobility of free and adsorbed shale oil can provide an important basis for the effective development of shale oil reservoirs, and the mobility of shale oil is closely related to the flow behavior of oil at the nanoscale (Zhang et al., 2019b; Zhu et al., 2023). MD studies of shale oil flow behavior under different nanopore types and reservoir conditions are summarized in Table 4. Elevating temperature usually enhances the thermal movement of shale oil molecules, thereby improving the flow capacity of oil molecules (Skoulidas et al., 2002; Liu et al., 2022a). The flow velocity profile of octane in graphene nanopores with strong adsorption capacity shows plug flows instead of the expected parabolic flow (Fig. 4(a)) (Falk et al., 2012; Wang et al., 2016a). This is because the ultrasmooth surface of graphene nanopores has minimal frictional resistance during the flow of oil molecules (Skoulidas et al., 2002), and the roughness of the wall has a greater impact on the flow capacity of oil than the adsorption of the wall. This conclusion was also confirmed in the studies of Falk et al.

(2012) and Asai et al. (2022). By contrast, the flow velocity distribution of hexane in silica nanotubes is parabolic, indicating that the flow capacity of oil molecules near the wall is relatively weak (Fig. 4(b)) (Asai et al., 2022). This is because the rough quartz wall has strong friction with oil molecules (Vinogradova and Yakubov, 2006).

The flow velocity and the flux of shale oil (Fig. 4(c)) increase as the displacement pressure gradient (DPG) increases (Sun et al., 2023c; Li et al., 2024). It should be noted that the velocity profile of shale oil changes from parabolic to piston type when the DPG exceeds the critical pressure gradient within the nanopore (Fig. 4(c)) (Sun et al., 2023c), and the increase in nanopore size also causes similar changes in the velocity profile of shale oil (Wang et al., 2016b). It can be observed from Fig. 4(d) that the shale oil flow exhibits positive slip near the quartz wall and negative slip near the kerogen wall (Li et al., 2024), resulting in a relatively large critical pressure gradient of kerogen nanopores (Sun et al., 2023c). Nanoporous media are closer to reality than slit and nanotube models, but hydrodynamics and Darcy's law fail to describe the hydrocarbon transport in nanoporous media because strong molecular adsorption can lead to non-viscous flow (Falk et al., 2015). The frictional effect of nanoporous media on hydrocarbon molecules is complex (Fig. 4(e)), but the flow velocity of hydrocarbon molecules is positively linearly correlated with the DPG (Fig. 4(f)) (Falk et al., 2015). In addition, many studies have shown that the permeability of shale oil in kerogen nanoporous media is inversely proportional to its adsorption amount (Collell et al., 2015; Falk et al., 2015; Obliger et al., 2016). Last but not least, all the research on porous media mentioned above is focused on kerogen, and further breakthroughs are needed in the construction of inorganic minerals nanoporous media.

4.2. Effects of shale oil components and formation water

The occurrence characteristics of different components of shale oil in nanopores and the presence of formation water with different salinities also affect the flow behavior of shale oil. It was reported that the penetration distance of shale oil with high heavy hydrocarbon content in the kerogen nanopores per unit time is the shortest because of the strong adsorption of heavy hydrocarbons by kerogen (Fig. 5(a)) (Sang et al., 2022). It reflects that the longer the molecular carbon chain, the weaker the flow capacity (Wang et al., 2023d). The number of aromatic and non-hydrocarbon molecules parallel to the wall surface is relatively fewer than that of saturated hydrocarbons, which increases the friction between the adsorbed and free phases of shale oil and hinders the flow of oil in the free phase (Wang et al., 2023d). Moreover, non-hydrocarbon such as naphthenic acid can form H-bongs with walls, and the electrostatic interaction between the two is extremely strong, which greatly hinders the flow of shale oil (Fig. 5(b)) (Wang et al., 2023d). It can be inferred that polar components are generally less mobile and more difficult to explore (Zhang et al., 2020). It is worth noting that all of the above factors may be reflected in asphaltenes, making the asphaltenes difficult to flow (Tinni et al., 2017; Wang et al., 2022a). Therefore, a sticky layer still exists on the kerogen surface in the presence of methane (Fig. 5(c)) (Wang et al., 2022a). The overall flow state shows that the velocity profile normal vector of shale oil at the kerogen matrix boundary is opposite to the velocity profile normal vector of the bulk phase (Fig. 5(d)), indicating that the flow velocity of shale oil in the kerogen nanopores presents hybrid heterogeneous distribution (Liu et al., 2022a). Furthermore, the bulk phase region and boundary region can be divided by the turning point of the shale oil shear rate in Fig. 5(e).

The flow state of shale oil in hydrated nanopores is more complex than the results shown in Fig. 5(d) (Zhan et al., 2020). The

Table 4MD studies of the flow behavior of shale oil.

Reference	Nanopore type	Force field	Temperature, K	Pressure gradient, MPa/nm	Research results
Liu et al. (2022a)	Kerogen (slit model)	PCFF+	300-420	4.76-23.78	Shale oil flow velocity increases with the increase of temperature.
Wang et al. (2016a)	Graphene (slit model)	OPLS-AA OPLS-UA	353-413	$(3.54-19.94) \times 10^{-2}$	The flow velocity profile of octane in smooth graphene nanopores is piston-shaped.
Falk et al. (2012)	Carbon (nanotube model)	OPLS	300	0.1	Shale oil flow velocities in carbon nanotubes are 1–3 orders of magnitude higher than those predicted from the continuum hydrodynamics framework and the no-slip boundary condition.
Asai et al. (2022)	Silica (nanotube model)	OPLS-AA CLAYFF	300	10	A linear relation between DPG and flow velocity can be observed when the DPG is over 10 MPa/nm.
Sun et al. (2023c)	Quartz and kerogen (slit model)	OPLS-AA CVFF CLAYFF	353	3–55	The critical pressure gradient for oil flow regimes changes in quartz nanopores is greater than that in kerogen nanopores.
Wang et al. (2016b)	Quartz (slit model)	OPLS CLAYFF	353–413	6.95-138.95	The velocity difference between free-phase molecules and adsorbed-phase molecules increases with the increase of nanopore size.
Li et al. (2024)	Quartz and kerogen (slit)	OPLS-AA CVFF CLAYFF	298-373	0.45-81.3	The negative slip of shale oil is caused by rough wall surfaces.
Falk et al. (2015)	Kerogen (nanoporous media)	OPLS-UA	423	≤100	Permeances are shown to follow an unexpected yet simple scaling with the alkane length.
Obliger et al. (2016)	Kerogen (nanoporous media)	OPLS	423	≤100	Permeances were found to decrease with the number of adsorbed molecules.

fluids in hydrated quartz nanopores are mainly divided into the oilphase zone, the oil—water boundary zone, and the near-wall water layer (Fig. 5(e)), and positive slip occurs in the AWIR (Zhang et al., 2021). In addition, the presence of water bridges in the nanopores hinders the flow of shale oil, which causes the velocity profile of shale oil to change into a piston type when the water content is high (Makimura et al., 2013). As mentioned earlier, brine can alter the wettability of charged calcite surfaces (Cooke et al., 2010; Zhao et al., 2019). Therefore, the water film on the calcite surface reduces the adsorption of the decane on the wall and improves the mobility of the decane (Fig. 5(f)) (Zhao et al., 2019). It should be noted that there is a positive slip phenomenon at the oil-brine interface similar to Fig. 5(e), and the increase in the thickness of the brine film can further promote the positive slip process (Fig. 5(g)) (Fang et al., 2019a). Generally, the reduction in nanopore size can lead to obstruction of shale oil flow (Jamin effect) (Falk et al., 2012). It should be emphasized that the exclusive effects of adsorbed hydrated Na⁺ ions on adsorbed water can lead to a reduction in the number of H-bongs between water molecules and illite, thereby reducing the water layer thickness (Fig. 5(h)) (Sedghi et al., 2016). As a result, the flow space of shale oil increases, and the influence of the Jamin effect on its flow capacity weakens (Sedghi et al., 2016). However, the oil-brine interfacial tension increases with increasing salinity, and therefore excessive salinity of brine can hinder the flow of shale oil (Xiong and Devegowda, 2022). In summary, an optimal amount of water with the appropriate salinity in nanopores can significantly facilitate shale oil flow. However, these are only for inorganic nanopores, and the effect of water or brine in organic nanopores on shale oil flow needs to be fully investigated.

5. CO₂-EOR mechanism of shale oil in nanopores

5.1. CO₂—shale oil interaction mechanisms in nanopores

CO₂ injection has been proven to be an effective method to enhance shale oil recovery because CO₂ not only has good injectability and mobility but also can exert multiple EOR mechanisms (Xiong et al., 2021; Wang et al., 2023e). The molecular diffusion, miscibility, and competitive adsorption mechanisms of CO₂ and

shale oil play an important role in the CO₂-EOR of shale oil reservoirs, which is also an important feature of shale reservoirs that is different from conventional reservoirs (Jia et al., 2019; Lashgari et al., 2019). CO₂ can diffuse into the nanopores of various mineral types to interact with shale oil, and then replace the free-phase oil molecules (Fig. 6(a)) (Takbiri-Borujeni et al., 2019). CO2 and shale oil can completely reach a miscible state when the pressure is greater than MMP (Fig. 6(b)) (Wu et al., 2016). The transformation of two-phase flow into single-phase flow and the variation in contact relationship between oil and walls effectively improve the mobility of shale oil in nanopores under miscible conditions (Huang et al., 2022; Wang et al., 2024). In addition, the interactions between CO_2 and kerogen and between CO_2 and n-dodecane are stronger than those between *n*-dodecane and kerogen with the simulation (Fig. 6(c)), and CO₂ can be dissolved in kerogen (Zhao et al., 2021a). This means that the competitive adsorption of CO₂ and oil on the wall can effectively improve the replacement effect of CO₂ on adsorbed and even dissolved shale oil (Dong et al., 2022a). CO₂-EOR mechanisms of shale oil reservoirs also include swelling, extraction, and viscosity reduction, which have been introduced in detail in our previous review (Wang et al., 2023a). The two mainstream methods of continuous CO₂ injection (CO₂ flooding) and periodic CO₂ injection (CO₂ huff-n-puff) were discussed separately in the following.

5.2. CO₂ flooding in nanopores

The displacement/replacement efficiency of CO₂ in nanopores is an important indicator to evaluate the effectiveness of CO₂ injection methods and the effect of CO₂-EOR (Zhao et al., 2021b). It was reported that the competitive adsorption of CO₂ and shale oil in montmorillonite nanopores is generally weaker than that in quartz and feldspar nanopores (Fig. 7(a)) (Dong et al., 2023b). However, the displacement effect of CO₂ on shale oil is better in montmorillonite nanopores than in quartz and feldspar nanopores because the surface of montmorillonite is relatively smooth (Dong et al., 2023b). Besides, adsorbed and dissolved shale oil in kerogen nanopores is difficult to be effectively displaced, but adsorbed shale oil in cristobalite nanopores is preferentially displaced, and the CO₂ flooding front morphology in the two nanopores is also

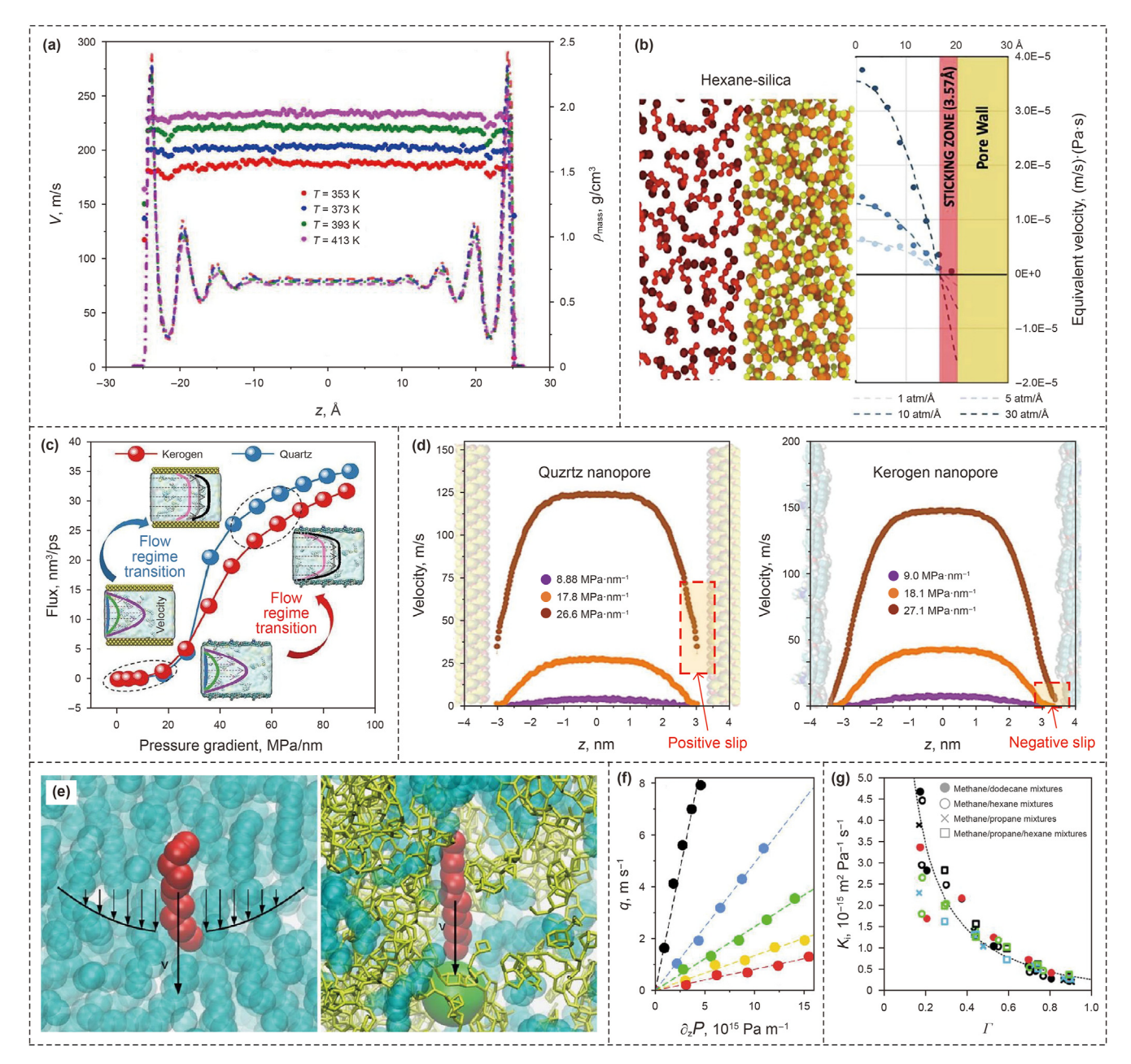


Fig. 4. Flow behavior of shale oil in different types of nanopores. (a) Flow velocity profile of octane in graphene nanopores under different temperatures (Wang et al., 2016a); (b) A snapshot of hexane—silica and flow velocity profile of hexane in quartz nanotubes under different DPG (Asai et al., 2022); (c) Flux of shale oil under different DPG and flow regime transition (Li et al., 2024); (d) Flow velocity profile of shale oil in quartz and kerogen nanopores under different DPG (Li et al., 2024); (e) Flow mechanisms of bulk alkanes (left) and alkanes confined in nanoporous media (right) (Falk et al., 2015); (f) Linear response of mean flow velocity of multiple oil components to DPG (black represents methane, blue represents propane, green represents hexane, yellow represents nonane and red represents dodecane) (Falk et al., 2015); (g) Permeability of different components in different mixtures as a function of the total loading (color code consistent with (f)) (Obliger et al., 2016).

significantly different (Fig. 7(b)) (Liu et al., 2017; Sui et al., 2023). For nanopores with different structures, the gradual reduction of pore size along the direction of CO₂ flooding can increase the displacement resistance, resulting in more residual oil in the pores (Fig. 7(c)) (Wang et al., 2022b). The CO₂ flooding process in multiple nanopores also indicates that variations in pore structure and size can limit the displacement effect of CO₂ (Fig. 7(d)) (Luo et al., 2023a). A large amount of CO₂ preferentially enters the mainstream channel, resulting in insufficient displacement of shale oil in small channels (Luo et al., 2023a, 2023b). However, these studies only constructed quartz walls, and there is a lack of MD research on CO₂ flooding behavior in porous media of clay minerals, organic

matter, and multiple mineral composites.

Compared with CO₂, N₂ has the advantages of sufficient supply, non-corrosiveness and low cost (Macintyre, 1986; Karim et al., 1992), and its favorable compression and expansion properties make N₂/CO₂ slug flooding (N₂ pushing CO₂ slug) more effective than CO₂—N₂ mixture flooding (Fischer et al., 1984; Fang et al., 2019b). One of the problems faced by CO₂ flooding is that excessive displacement pressure or injection velocity can lead to severe gas channeling, resulting in more residual oil in nanopores (Dong et al., 2023b; Sui et al., 2023), and the addition of N₂ may exacerbate this problem (Si et al., 2024). In addition, natural gas as produced gas can also be injected into shale reservoirs to enhance oil

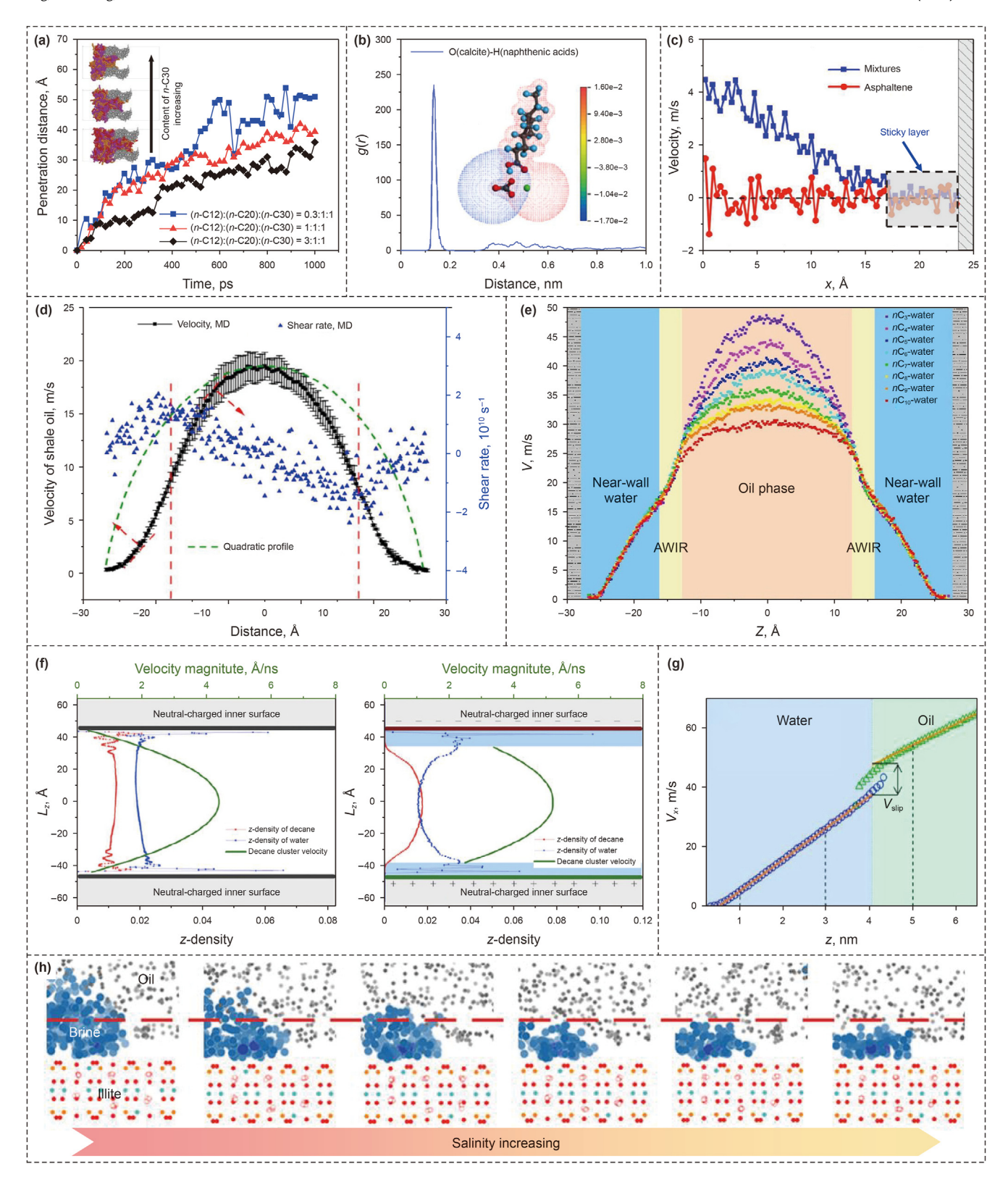


Fig. 5. Flow behavior of shale oil with different components in nanopores. (**a**) Variation of penetration distance with time of different alkane ratios in kerogen nanopores (**Sang** et al., 2022); (**b**) RDF and electrostatic interaction between naphthenic acid and calcite surface (Wang et al., 2023d); (**c**) Velocity profiles of hydrocarbon mixtures (methane + octane + asphaltene) and asphaltene in kerogen nanopore (Tian et al., 2018); (**d**) Flow velocity profile and shear rate distribution of shale oil in kerogen nanopores (Liu et al., 2022a); (**e**) Flow velocity profiles of *n*-alkanes and water in quartz nanopores (Xu et al., 2022b); (**f**) *n*-decane velocity profiles in neutral surface—brine system (left) and charged surface—brine system (right) (Zhao et al., 2019); (**g**) Flow velocity profiles of water and decane (Fang et al., 2019a); (**h**) Distribution of brine and oil with different salinities (Sedghi et al., 2016).

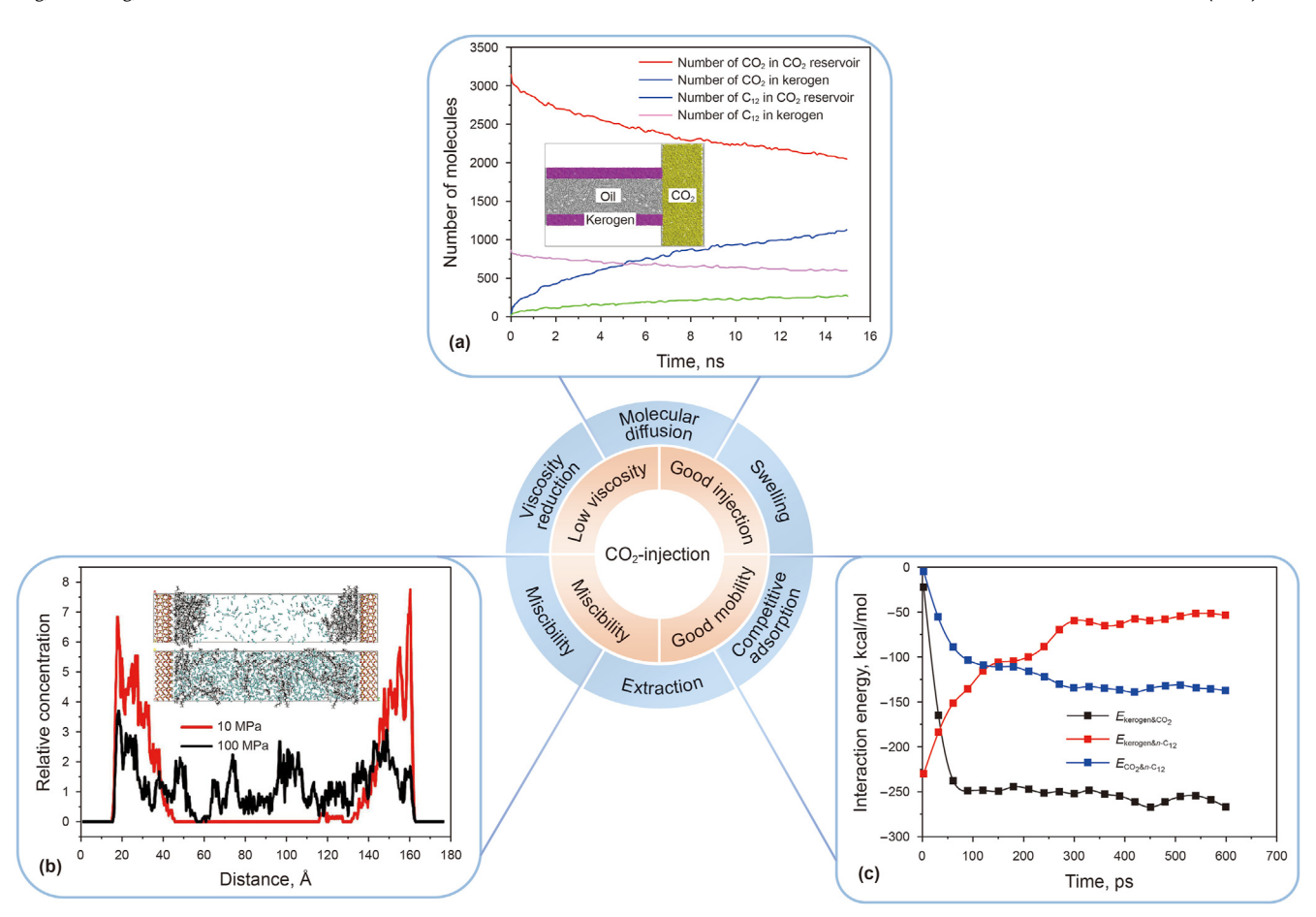


Fig. 6. CO₂-EOR mechanisms. (**a**) Variations of molecular number with time in kerogen nanochannel and CO₂ container (Takbiri-Borujeni et al., 2019); (**b**) Configurations and concentration distributions of dodecane in nanopores at different pressures (Wu et al., 2016); (**c**) Interaction energies of kerogen—CO₂, kerogen—*n*-dodecane and CO₂—*n*-dodecane in nanopores (Zhao et al., 2021a).

recovery. It was reported that N₂ and CH₄ are more prone to gas channeling by comparing the four gases of CO₂, CH₄, N₂, and C₃H₈ (Fig. 7(e)), resulting in lower displacement efficiency (Xiong et al., 2021). CO₂ and C₃H₈ are well miscible with shale oil (Li et al., 2020d), and the competitive adsorption of CO₂-oil and C₃H₈-oil on the rock wall is strong, which improves the displacement efficiency of both (Xiong et al., 2021). The presence of water bridges in nanopores can create resistance to CO2 flooding, but CO2 can destroy the H-bongs between water molecules in the center of the water bridge (CWB), thereby breaking through the water bridge and recovering shale oil (Fig. 7(f)) (Liu et al., 2022b). It is worth noting that the addition of hydrocarbon gases can reduce the oil—water IFT and enhance the mobility of shale oil (Fig. 7(g)) (Zhang et al., 2023b). Therefore, mixing hydrocarbon gases with CO₂ may promote CO₂ flooding to overcome the negative effects of water bridges and enhance competitive adsorption, thereby further enhancing oil recovery.

5.3. CO₂ huff-n-puff in nanopores

Field tests have shown that CO₂ flooding in shale oil reservoirs causes severe gas channeling, which affects the sweep range of CO₂ and the contact time between CO₂ and oil (Liu and Zhang, 2015; Zhang et al., 2023b). By contrast, full contact between CO₂ and oil can promote the miscibility of the two phases through molecular diffusion and extract adsorbed oil in the nanopores through the "soaking" process of CO₂ huff-n-puff (Hawthorne et al., 2013; Teklu

et al., 2014). Previous studies have shown that CO2 replacement efficiency from high to low is calcite, montmorillonite, feldspar, quartz, and graphene (Dong et al., 2023a). This means that the competitive adsorption of CO2 and oil on calcite walls is the strongest, which also explains why CO₂ moves along the calcite wall (Fig. 8(a)) (Moh et al., 2022). Increases in temperature and pore size can weaken the adsorption of oil molecules on the wall, while an increase in pressure can promote the miscibility of CO₂ and shale oil (Archer et al., 2003; Adel et al., 2018). Therefore, the replacement efficiency of CO₂ huff-n-puff in the dead-end graphene nanopores is positively correlated with temperature, pressure, and pore size (Sun et al., 2023b). In addition, the depressurization process after soaking is crucial to EOR, and there is an optimal depressurizing rate. An excessively high depressurizing rate shortens the duration of the entire pressure drop process, while an excessively low depressurizing rate reduces the extraction force. The above two factors are not conducive to oil extraction (Fig. 8(b)) (Fang et al., 2020). It needs to be emphasized that the mutual solubility of CO₂ and oil weakens as the pressure decreases, causing some oil molecules to re-absorb on the pore wall (Fig. 8(c)). However, the applicability of the series of laws obtained from the above investigations in the kerogen pores still needs further verification.

The blocking effect of water film on shale oil in dead-end nanopores increases its extraction resistance, but CO_2 can still replace it. CO_2 molecules continuously dissolve in water and diffuse into the oil phase, and the water film is eventually broken accompanied by the continuous expansion of the shale oil volume

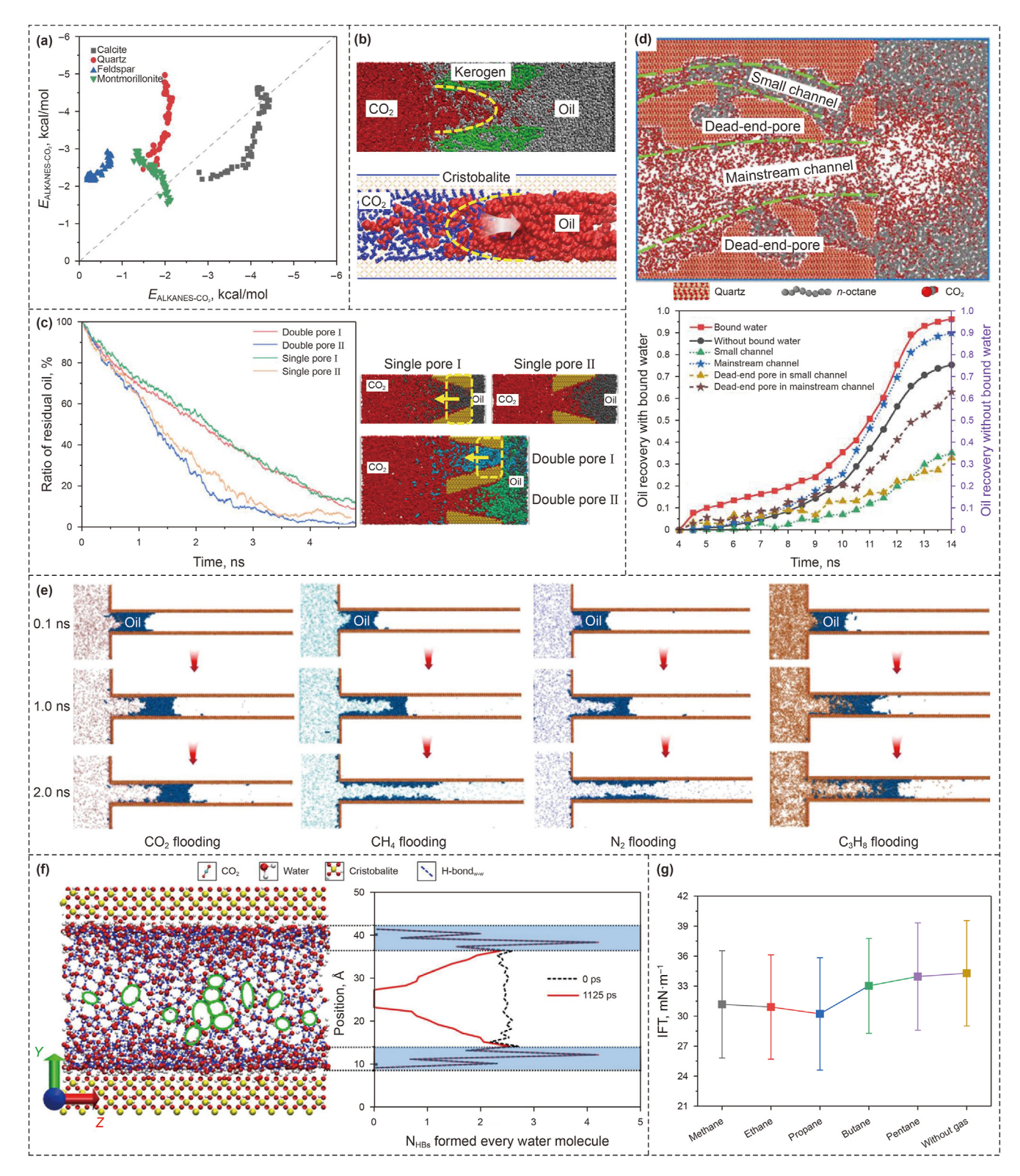


Fig. 7. MD simulation results of continuous CO₂ injection. (a) Interaction energy of oil—CO₂ and oil—wall (Dong et al., 2023b); (b) Snapshots of CO₂ flooding in kerogen nanopores and cristobalite cylindrical nanopores (Liu et al., 2017; Sui et al., 2023); (c) The ratio of residual oil in nanopores and snapshots of CO₂ flooding in single and double pores (Wang et al., 2022b); (d) Displacement efficiency and final snapshot of CO₂ flooding in multiple nanopores (Luo et al., 2023a); (e) CO₂, CH₄, N₂, and C₃H₈ flooding processes (Xiong et al., 2021); (f) Snapshots of the initial H-bongs distribution and the average number of H-bonds in the y-direction in nanopores (Liu et al., 2022b); (g) Oil—water IFT values after adding different hydrocarbon gases (Zhang et al., 2023b).

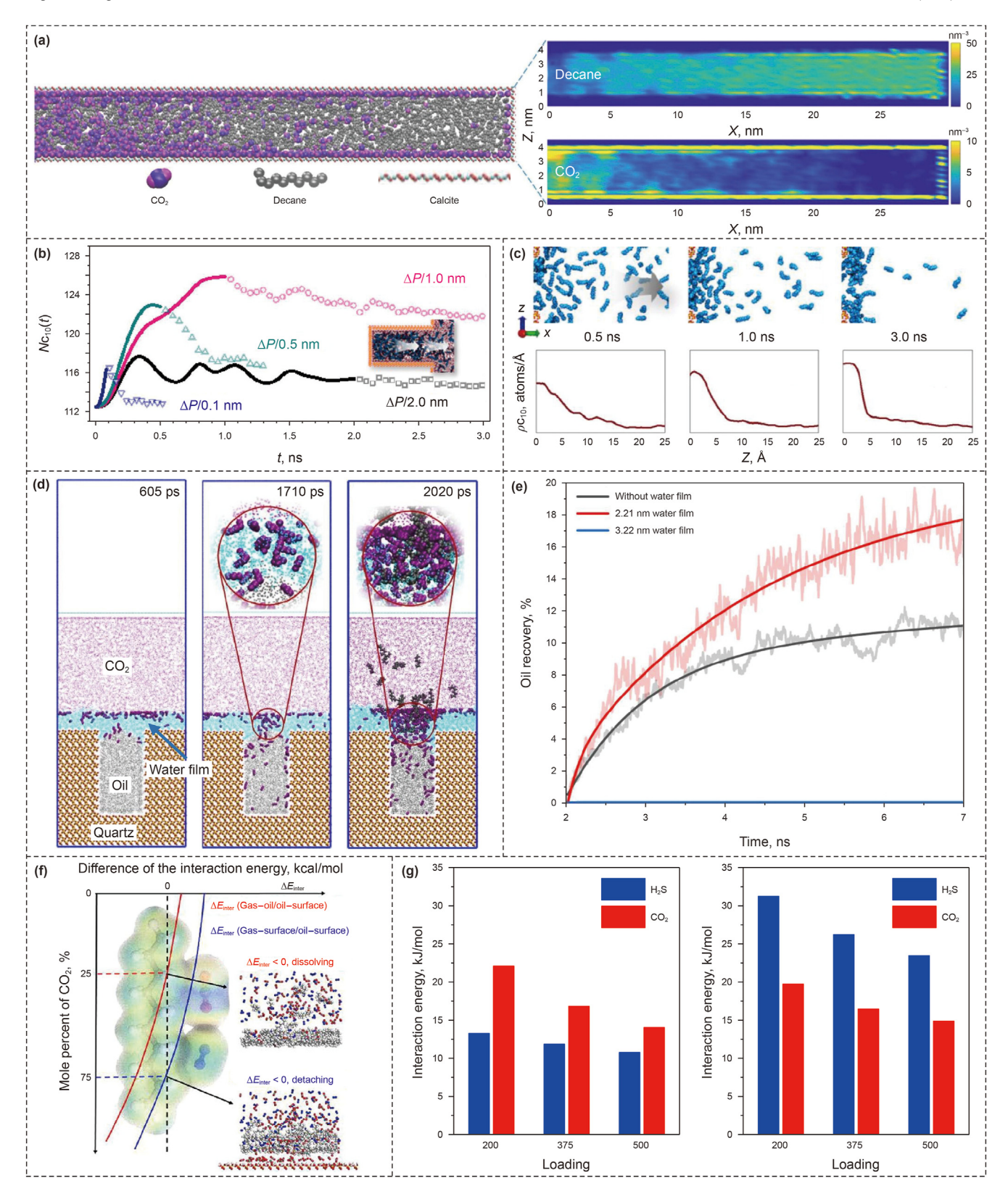


Fig. 8. MD simulation results of CO₂ huff-n-puff. (a) Density evolution of decane and CO₂ in calcite nanopores (Moh et al., 2022); (b) Extraction results of *n*-decane with different depressurization rate, solid line: extract period, dotted line: equilibrium period (Fang et al., 2020); (c) Side views for the evolutions and density profiles outside the nanopore (Fang et al., 2020); (d) Snapshots of replacement of oil by CO₂ in quartz dead-end nanopores (Luan et al., 2020); (e) Oil recovery factor under different water film thicknesses (Luo et al., 2023b); (f) Differences in interaction energy of gas—oil/oil-surface and gas-surface/oil-surface (Yu et al., 2022); (g) Magnitude of total interaction energy of CO₂ and H₂S at different loadings for silica (left) and muscovite (right) (Badmos et al., 2019).

(Fig. 8(d)) (Luan et al., 2020). Subsequently, CO₂ is directly contact with shale oil to achieve oil replacement. However, the increase of water film thickness can hinder the extraction of shale oil by CO₂, resulting in a decrease in oil recovery (Fig. 8(e)) (Luo et al., 2023b). It needs to be emphasized that the excessive thickness of the water film can prevent CO₂ from penetrating the water film, making it difficult for the oil inside the pores to be replaced (Bijeljic et al., 2002; Luo et al., 2023b). CO₂ usually contains impurity gases in the actual development process, which cannot be ignored in MD simulation studies. N2 is immiscible with shale oil and there is no competitive adsorption between the two. Therefore, a CO₂-N₂ mixture with a 75% molar percentage of CO₂ is required to effectively strip the oil film adsorbed on the quartz wall (Fig. 8(f)) (Yu et al., 2022). In addition, acidic gases such as H₂S are also common impurity gases in impure CO2. It was reported that the CO2-H2S mixture is more suitable for replacing shale oil in muscovite than in quartz nanopores. This is because muscovite has a relatively strong adsorption effect on H₂S (Fig. 8(g)), which promotes the competitive adsorption between oil and gas phases (Badmos et al., 2019). However, the effect of H₂S concentration on the microscopic mechanisms of CO₂-EOR is not yet clear, and there is still a lack of MD studies on other types of impurity gases.

6. Challenges and perspectives

6.1. Spatial and temporal scales of MD simulations

MD simulations are commonly used to conduct various studies of fluids in individual nanopores. However, this simplified method makes it difficult to reflect the strong heterogeneity of shale reservoirs. Therefore, constructing porous media models that are closer to actual reservoirs is still one of the main challenges faced by MD technique at present. The duration of actual physical and chemical processes far exceeds the time scale that MD technique can simulate. Therefore, MD technique still has technical difficulties in simulating long-term processes such as cross-scale fluid flow, gas huff-n-puff, and CO₂ geological storage.

Therefore, it is necessary to innovate the idea of simulation. Considering that some micro-phenomena are rare, the probability of rare events can be increased by changing certain conditions of MD simulations. More importantly, it is urgent to develop a set of universally accepted standards for MD simulation to guide the construction of pore and fluid models and the calculation of microscopic parameters. In addition, dissipative particle dynamics (DPD) significantly reduces computational demands by coarsegrained multiple atoms into one particle. Consequently, this method can typically reach spatial scales of tens of micrometers and time scales of several microseconds, which can compensate for the current situation that MD methods cannot study the mesoscopic fluid behavior in shale reservoirs. The fluid parameters (adsorption layer thickness and density, diffusion coefficient, etc.) obtained by MD can also be substituted into the Lattice Boltzmann method (LBM) and pore network model (PNM). The nanoscale effect can be considered in pore-scale simulations by modifying the parameters of boundary conditions or flow equations (analytical models). It is noteworthy that machine learning can also extend MD results to macroscopic spatial and temporal scales. The random forest machine learning algorithm extracts key features (molecular conformational features, energy parameters, etc.) from MD simulation data and performs normalization and standardization. The trained random forest model can extend MD results to core-scale applications. The Markov state model can discretize the continuous motion of the system obtained from MD simulations into a series of states. It enables the prediction of dynamical behavior that extend far beyond the actual MD simulation time by constructing

transition probability matrices for these discrete states. Continuously promoting the organic combination of the above methods with MD simulations can effectively achieve up-scaling of MD results.

6.2. Realistic and complexity of MD simulations

Most MD studies use a single mineral and component to represent the rock wall and shale oil separately, which inevitably leads to significant differences between simulations and realities. More importantly, there are complex chemical reactions in shale reservoirs during oil extraction and carbon storage, and the classical MD method cannot consider the formation and breakage of chemical bonds. This limitation to some extent affects the application scope and accuracy of MD technique.

Therefore, constructing multi-mineral composite pore walls and multi-component composite shale oil can make MD simulation results closer to reality. Various minerals can be mixed or assembled in different ways to construct nanopore models with anisotropic characteristics. Scenarios involving chemical reactions in shale reservoir research can be broadly categorized into four areas. The first area involves the pyrolysis of kerogen and the reaction between formation water and rock minerals during the accumulation process. The second area is the reaction between fracturing fluids and shale matrix during the hydraulic fracturing process. The third area involves the reaction between CO₂ and organic matter in the process of CO₂ injection. The fourth area is the formation of precipitates in the process of CO₂ mineralization. The system needs to be divided into reactive regions (handled by ReaxFF) and nonreactive regions (handled by classical MD force fields) to the study above chemical reaction processes. It is crucial to ensure a smooth transition between the two regions at the boundary (handled by ReaxFF and classical MD force fields collaboratively) (Rahnamoun et al., 2020). Electrostatic interactions between ReaxFF-ReaxFF/molecular mechanics (MM) atomic pairs are calculated by ReaxFF. The van der Waals interactions between ReaxFF–ReaxFF/MM atomic pairs are handled by classical MD force fields. Chemical and non-chemical processes occur simultaneously and exchange information at their boundary. Currently, ReaxFF has been applied to the study of kerogen pyrolysis, water-rock interactions, and multiphase fluid reactions in shale reservoirs. However, there has not yet been a combination of ReaxFF and classical MD force fields in shale reservoir studies. The possible reason is that ReaxFF is still not suitable for large-scale systems. Advancing this technology can significantly enhance the investigation of chemical reactions in fluid behavior and EOR mechanisms of shale oil, thereby making simulation results more reflective of actual conditions.

6.3. Verification and application of MD simulations

MD simulation results inevitably have certain systematic errors under the influence of various simplifications and uncertainties in assumptions, boundary conditions, and force fields. Therefore, it is necessary to further verify the MD results in combination with other techniques. However, the verification of MD simulation results is extremely difficult because some microscopic parameters are difficult to determine through experiments and numerical simulations. In addition, MD simulations at the microscale are conducted under relatively ideal conditions, whereas reservoir exploitation needs to consider complex formation conditions, as well as equipment limitations, implementation difficulties, and economic benefits. Therefore, the results obtained through MD simulation are difficult to directly apply to oilfield exploitation, which limits the application and development of MD technique.

Although the systematic error of MD simulation cannot be avoided, the accuracy can be improved by the reduced statistical error by constructing reasonable initial configurations, increasing simulation frequency, and extending simulation time. Although some microscopic mechanisms obtained by MD simulation cannot be verified by experiments, the accuracy of MD simulation results can be proved by comparing fluid parameters such as density. viscosity, diffusion coefficient and, IFT that can be obtained by both methods. Mutual verification of MD simulation and laboratory experimental results can not only ensure the accuracy of research results but also promote the integrated development of the two techniques. Importantly, the parameters obtained from MD simulation can be used to optimize experimental parameters (e.g. fluid properties, thermodynamic, and injection/production parameters) and improve mathematical models (e.g. fluid flow, phase behavior, and heat and mass transfer models) for their applications at the macroscale. In addition, the microscopic mechanisms derived from MD simulations can be used to elucidate phenomena and patterns (e.g. slip flow near walls, interfacial phenomena, phase transitions, and molecular diffusion) that are challenging to interpret through experiments and numerical simulations, thereby enhancing the macroscopic significance of MD results.

7. Conclusions

MD simulations can quantitatively characterize various fluid properties, flow characteristics, and action mechanisms at the nanoscale. Therefore, the current application status of MD simulation in shale oil occurrence characteristics, flow behavior, and EOR methods was reviewed, and reasonable prospects were proposed based on the existing challenges.

- (1) The core of MD simulation is the force field, and the force fields applicable to various materials under different scenario are different. Appropriate force field selection can not only improve the accuracy of simulation results but also reduce the computational cost. Considering the characteristics of the NVT and NPT ensembles, it is preferable to equilibrate system temperature and pressure in separate steps. As force fields and ensembles are continually refined, their accuracy has significantly improved and their applicability has been expanded. This advancement enables MD simulations to address increasingly diverse scientific questions. Furthermore, methods for calculating static, dynamic, and interfacial parameters of fluids have been developed, which can be used to characterize the occurrence characteristics, hydrodynamic properties and interface properties of shale oil during reservoir exploitation.
- (2) MD simulations have been widely applied in the study of shale oil reservoirs, and the factors involved include reservoir conditions, fluid properties, nanopore types, inorganic salt ions, and injection/production parameters. Regarding the occurrence characteristics of shale oil, research on the occurrence of multicomponent fluids within composite mineral nanopores has been achieved. However, the combination of various minerals in these composite nanopores tends to be relatively simple and idealized, and research on organic nanopores remains incomplete. Regarding the flow behavior of shale oil, distinct flow states of oil have been identified in both slit and matrix pores. However, the construction of inorganic mineral nanoporous media still requires further breakthroughs. Regarding the CO2-EOR in shale reservoirs, MD simulations are primarily used to study the effect of CO₂ on the mobilization of shale oil in various types of nanopores. MD simulations of different CO2

- injection methods aid in the optimization of oilfield development schemes. Additionally, accurate simulation of novel or improved gas injection methods is one of the future directions for the application of MD methods.
- (3) The main challenges faced by MD simulation on shale reservoirs include limited spatial and temporal scales, insufficient simulation realism and complexity, and difficulty in verification and application. Furthermore, the simulation of chemical reactions requires further advancement in the integration of ReaxFF with MD force fields. It is unrealistic to solve practical engineering problems only by MD, which requires a combination of multiple research methods. LBM, PNM, and machine learning can achieve the upscaling of MD results. Physical simulation experiments and reservoir numerical simulations are not only crucial methods for studying macroscopic phenomena, but also essential options for validating MD results. The organic integration of multi-scale research methods is an important future development trend in shale reservoir studies.

CRediT authorship contribution statement

Lu Wang: Writing — original draft, Resources, Project administration, Methodology, Funding acquisition, Conceptualization. **Yi-Fan Zhang:** Writing — original draft, Resources, Investigation, Formal analysis, Data curation. **Run Zou:** Writing — original draft, Formal analysis, Data curation. **Yi-Fan Yuan:** Investigation, Formal analysis, Data curation. **Rui Zou:** Investigation, Formal analysis, Data curation. **Liang Huang:** Resources, Funding acquisition, Conceptualization. **Yi-Sheng Liu:** Supervision, Resources, Formal analysis. **Jing-Chen Ding:** Supervision, Methodology, Funding acquisition. **Zhan Meng:** Supervision, Resources, Project administration, Methodology, Conceptualization.

Declaration of competing interest

The authors declare that they have no known competing financial interests or personal relationships that could have appeared to influence the work reported in this paper.

Acknowledgement

This paper was supported by the National Natural Science Foundation of China (52304021, 52104022, 52204031), the Natural Science Foundation of Sichuan Province (2022NSFSC0205, 2024NSFSC0201, 2023NSFSC0947), and the National Science and Technology Major Projects of China (2017ZX05049006-010). Furthermore, we would like to thank Dr. Xingli Xu for her valuable suggestions and support for this paper.

Appendix A. Supplementary data

Supplementary data to this article can be found online at https://doi.org/10.1016/j.petsci.2024.09.023.

References

Adel, I.A., Tovar, F.D., Zhang, F., et al., 2018. The impact of MMP on recovery factor during CO₂—EOR in unconventional liquid reservoirs. In: SPE Annual Technical Conference and Exhibition. https://doi.org/10.2118/191752-MS.

Allen, W., Rowley, R.L., 1997. Predicting the viscosity of alkanes using nonequilibrium molecular dynamics: evaluation of intermolecular potential models. J. Chem. Phys. 106 (24), 10273–10281. https://doi.org/10.1063/1.474052.

Andersen, H.C., 1980. Molecular dynamics simulations at constant pressure and/or temperature. J. Chem. Phys. 72 (4), 2384–2393. https://doi.org/10.1063/ 1.439486.

Archer, T.D., Birse, S.E.A., Dove, M.T., et al., 2003. An interatomic potential model for carbonates allowing for polarization effects. Phys. Chem. Miner. 30, 416–424. https://doi.org/10.1007/s00269-002-0269-z.

- Asai, P., Jin, J., Deo, M., et al., 2022. Non-equilibrium molecular dynamics simulation to evaluate the effect of confinement on fluid flow in silica nanopores. Fuel 317, 123373. https://doi.org/10.1016/j.fuel.2022.123373.
- Badmos, S.B., Bui, T., Striolo, A., et al., 2019. Factors governing the enhancement of hydrocarbon recovery via H₂S and/or CO₂ injection: insights from a molecular dynamics study in dry nanopores. J. Phys. Chem. C 123 (39), 23907–23918. https://doi.org/10.1021/acs.jpcc.9b04247.
- Badwaik, P., Chobe, S., Malani, A., 2023. Investigation of light oil—rock interactions using molecular dynamics simulations. Energy Fuels 37 (20), 15523–15536. https://doi.org/10.1021/acs.energyfuels.3c02424.
- Berendsen, H.J., Grigera, J.R., Straatsma, T.P., 1987. The missing term in effective pair potentials. J. Phys. Chem. 91 (24), 6269–6271. https://doi.org/10.1021/j100308a038.
- Bijeljic, B.R., Muggeridge, A.H., Blunt, M.J., 2002. Effect of composition on water-blocking for multicomponent gasfloods. In: SPE Annual Technical Conference and Exhibition. https://doi.org/10.2118/77697-MS.
- Botan, A., Rotenberg, B., Marry, V., et al., 2011. Hydrodynamics in clay nanopores. J. Phys. Chem. C 115 (32), 16109–16115. https://doi.org/10.1021/jp204772c.
- Cao, Z., Jiang, H., Zeng, J.H., et al., 2021. Nanoscale liquid hydrocarbon adsorption on clay minerals: a molecular dynamics simulation of shale oils. Chem. Eng. J. 420, 127578. https://doi.org/10.1016/j.cej.2020.127578.
- Chen, X.H., Zhang, M., 2017. Composition characteristics of the saturated hydrocarbon of the sequential extracts from the oil-bearing shale with different polarity reagents. Pet. Geol. Oilfield Dev. Daqing 36 (3), 168–174. In Chinese.
- Collell, J., Galliero, G., Vermorel, R., et al., 2015. Transport of multicomponent hydrocarbon mixtures in shale organic matter by molecular simulations. J. Phys. Chem. C 119 (39), 22587–22595. https://doi.org/10.1021/acs.jpcc.5b07242.
- Cooke, D.J., Gray, R.J., Sand, K.K., et al., 2010. Interaction of ethanol and water with the {1014} surface of calcite. Langmuir 26 (18), 14520—14529. https://doi.org/10.1021/la100670k.
- Cygan, R.T., Liang, J.J., Kalinichev, A.G., 2004. Molecular models of hydroxide, oxyhydroxide, and clay phases and the development of a general force field. J. Phys. Chem. B 108 (4), 1255–1266. https://doi.org/10.1021/jp0363287.
- Dai, X.G., Wei, C.T., Wang, M., et al., 2023. Understanding CO₂ mineralization and associated storage space changes in illite using molecular dynamics simulation and experiments. Energy 283, 128467. https://doi.org/10.1016/j.jenergy.2023.128467.
- Dash, B., Rath, S.S., 2020. Density functional theory and molecular dynamics insights into the site-dependent adsorption of hydrogen fluoride on kaolinite. J. Mol. Liq. 299, 112265. https://doi.org/10.1016/j.molliq.2019.112265.
- Dauber-Osguthorpe, P., Roberts, V.A., Osguthorpe, D.J., et al., 1988. Structure and energetics of ligand binding to proteins: Escherichia coli dihydrofolate reductase-trimethoprim, a drug-receptor system. Proteins: Struct., Funct., Bioinf. 4 (1), 31–47. https://doi.org/10.1002/prot.340040106.
- Donadelli, J.A., Canneva, A., Erra, G., et al., 2019. XPS direct analysis on shale rocks: correlation with kerogen type and maturity. Fuel 257, 116004. https://doi.org/10.1016/j.fuel.2019.116004.
- Dong, M.Z., Gong, H.J., Sang, Q., et al., 2022a. Review of CO₂-kerogen interaction and its effects on enhanced oil recovery and carbon sequestration in shale oil reservoirs. Resources Chemicals and Materials 1 (1), 93–113. https://doi.org/10.1016/j.recm.2022.01.006.
- Dong, X.H., Xu, W.J., Liu, R.J., et al., 2022b. Insights into adsorption and diffusion behavior of shale oil in slit nanopores: a molecular dynamics simulation study. J. Mol. Liq. 359, 119322. https://doi.org/10.1016/j.molliq.2022.119322.
- Dong, X.H., Xu, W.J., Liu, H.Q., et al., 2023a. On the replacement behavior of CO₂ in nanopores of shale oil reservoirs: insights from wettability tests and molecular dynamics simulations. Geoenergy Science and Engineering 223, 211528. https://doi.org/10.1016/j.geoen.2023.211528.
- Dong, X.H., Xu, W.J., Liu, H.Q., et al., 2023b. Molecular insight into the oil displacement mechanism of CO₂ flooding in the nanopores of shale oil reservoir. Petrol. Sci. https://doi.org/10.1016/j.petsci.2023.08.006.
- Du, M., Lyu, W.F., Yang, Z.M., et al., 2023. An online physical simulation method for enhanced oil recovery by air injection in shale oil. Petrol. Explor. Dev. 50 (4), 909–923. https://doi.org/10.1016/S1876-3804(23)60437-9.
- Dubey, S.T., Waxman, M.L., 1991. Asphaltene adsorption and desorption from mineral surfaces. SPE Reservoir Eng. 6 (3), 389–395. https://doi.org/10.2118/ 18462-PA.
- Einstein, A., 1905. Über die von der molekularkinetischen Theorie der Wärme geforderte Bewegung von in ruhenden Flüssigkeiten suspendierten Teilchen. Ann. Phys. 4. http://sedici.unlp.edu.ar/handle/10915/2785.
- Falk, K., Sedlmeier, F., Joly, L., et al., 2012. Ultralow liquid/solid friction in carbon nanotubes: comprehensive theory for alcohols, alkanes, OMCTS, and water. Langmuir 28 (40), 14261–14272. https://doi.org/10.1021/la3029403.
- Falk, K., Coasne, B., Pellenq, R., et al., 2015. Subcontinuum mass transport of condensed hydrocarbons in nanoporous media. Nat. Commun. 6 (1), 6949. https://doi.org/10.1038/ncomms7949.
- Fang, C., Sun, S.Y., Qiao, R., 2019a. Structure, thermodynamics, and dynamics of thin brine films in oil—brine—rock systems. Langmuir 35 (32), 10341–10353. https:// doi.org/10.1021/acs.langmuir.9b01477.
- Fang, T.M., Wang, M.H., Gao, Y., et al., 2019b. Enhanced oil recovery with CO₂/N₂ slug in low permeability reservoir: molecular dynamics simulation. Chem. Eng. Sci. 197, 204–211. https://doi.org/10.1016/j.ces.2018.12.016.

Fang, T.M., Zhang, Y.N., Yan, Y.G., et al., 2020. Molecular insight into the oil extraction and transport in CO₂ flooding with reservoir depressurization. Int. J. Heat Mass Tran. 148, 119051. https://doi.org/10.1016/i.jiiheatmasstransfer.2019.119051.

- Fei, J.S., Wang, M., Li, J.B., et al., 2023. Molecular dynamics simulation of adsorption and absorption behavior of shale oil in realistic kerogen slits. Energy Fuels 37 (5), 3654–3671. https://doi.org/10.1021/acs.energyfuels.2c03842.
- Fischer, D.D., Bilhartz, D., Holt, C., et al., 1984. Response of North Cowden and Goldsmith crudes to carbon dioxide slugs pushed by nitrogen. J. Petrol. Technol. 36 (1), 96–100. https://doi.org/10.2118/9719-PA.
- Frenkel, D., Smit, B., 2002. Understanding Molecular Simulations: From Algorithms to Applications. Chemical Industry Press. https://doi.org/10.1016/B978-012267351-1/50012-2.
- Gant, P.L., Anderson, W.G., 1988. Core cleaning for restoration of native wettability. SPE Form. Eval. 3 (1), 131–138. https://doi.org/10.2118/14875-PA.
- Gong, H.J., Lv, W., Zhang, H., et al., 2024. The influence and mechanism of alkyl block polyethers on the interfacial tension and minimum miscibility pressure of CO₂ and shale oil. Fuel 356, 129568. https://doi.org/10.1016/j.fuel.2023.129568.
- Green, M.S., 1952. Markoff random processes and the statistical mechanics of time-dependent phenomena. J. Chem. Phys. 20 (8), 1281–1295. https://doi.org/10.1063/1.1700722.
- Haile, J.M., 1992. Molecular Dynamics Simulation: Elementary Methods. John Wiley & Sons. Inc.
- Haile, J.M., Johnston, I., Mallinckrodt, A.J., et al., 1993. Molecular dynamics simulation: elementary methods. Comput. Phys. 7 (6). https://doi.org/10.1063/1.4823234, 625-625.
- Harris, J.G., Yung, K.H., 1995. Carbon dioxide's liquid-vapor coexistence curve and critical properties as predicted by a simple molecular model. J. Phys. Chem. 99 (31), 12021–12024. https://doi.org/10.1021/j100031a034.
- Hawthorne, S.B., Gorecki, C.D., Sorensen, J.A., et al., 2013. Hydrocarbon mobilization mechanisms from upper, middle, and lower Bakken reservoir rocks exposed to CO₂. In: SPE Unconventional Resources Conference Canada. https://doi.org/ 10.2118/167200-MS.
- Herdes, C., Petit, C., Mejía, A., et al., 2018. Combined experimental, theoretical, and molecular simulation approach for the description of the fluid-phase behavior of hydrocarbon mixtures within shale rocks. Energy Fuels. 32 (5), 5750–5762. https://doi.org/10.1021/acs.energyfuels.8b00200.
- Ho, T.A., Wang, Y.F., 2019. Enhancement of oil flow in shale nanopores by manipulating friction and viscosity. Phys. Chem. Chem. Phys. 21 (24), 12777–12786. https://doi.org/10.1039/C9CP01960J.
- Hockney, R.W., Eastwood, J.W., 2021. Computer Simulation Using Particles. CRC Press. https://doi.org/10.1201/9780367806934.
- Hu, S.Y., Zhao, W.Z., Hou, L.H., et al., 2020. Development potential and technical strategy of continental shale oil in China. Petrol. Explor. Dev. 47 (4), 819–828. https://doi.org/10.1016/S1876-3804(20)60103-3.
- Huang, L., Zhou, W., Xu, H., et al., 2021. Dynamic fluid states in organic-inorganic nanocomposite: implications for shale gas recovery and CO₂ sequestration. Chem. Eng. J. 411, 128423. https://doi.org/10.1016/j.cej.2021.128423.
- Huang, T., Cheng, L.S., Jia, Z.H., et al., 2023. Adsorption layer of complex oil components in organic-rich shale: a molecular dynamics simulation study. Geoenergy Science and Engineering 211987. https://doi.org/10.1016/j.geoen.2023.211987.
- Huang, X., Li, X., Zhang, Y., et al., 2022. Microscopic production characteristics of crude oil in nano-pores of shale oil reservoirs during CO₂ huff and puff. Petrol. Explor. Dev. 49 (3), 636–643. https://doi.org/10.1016/S1876-3804(22)60053-3.
- Huang, X., Yu, X., Li, X., et al., 2024. A review of the flow characteristics of shale oil and the microscopic mechanism of CO₂ flooding by molecular dynamics simulation. Front. Earth Sci. 12, 1401947. https://doi.org/10.3389/ feart.2024.1401947.
- IEA, 2023. Oil Market Report-June 2023. IEA, Paris. https://www.iea.org/reports/oil-market-report-june-2023.
- Jacobs, T., 2016. EOR-for-shale ideas to boost output gain traction. J. Petrol. Technol. 68 (6), 28–31. https://doi.org/10.2118/0616-0028-JPT.
- Jia, B., Tsau, J.S., Barati, R., 2019. A review of the current progress of CO₂ injection EOR and carbon storage in shale oil reservoirs. Fuel 236, 404–427. https://doi.org/10.1016/j.fuel.2018.08.103.
- Jiao, F.Z., Zou, C.N., Yang, Z., 2020. Geological theory and exploration & development practice of hydrocarbon accumulation inside continental source kitchens. Petrol. Explor. Dev. 47 (6), 1067–1078. https://doi.org/10.1016/S1876-3804(20) 60125-8.
- Jorgensen, W.L., Chandrasekhar, J., Madura, J.D., et al., 1983. Comparison of simple potential functions for simulating liquid water. J. Chem. Phys. 79 (2), 926–935. https://doi.org/10.1063/1.445869.
- Jorgensen, W.L., Maxwell, D.S., Tirado-Rives, J., 1996. Development and testing of the OPLS all-atom force field on conformational energetics and properties of organic liquids. J. Am. Chem. Soc. 118 (45), 11225—11236. https://doi.org/ 10.1021/ja9621760.
- Karim, F., Berzins, T.V., Schenewerk, P.A., et al., 1992. Light oil recovery from cyclic CO₂ injection: influence of drive gas, CO₂ injection rate, and reservoir dip. In: SPE Rocky Mountain Petroleum Technology Conference/Low-Permeability Reservoirs Symposium. https://doi.org/10.2118/24336-MS.
- Kim, C., Devegowda, D., 2022. Molecular dynamics study of fluid-fluid and solid-fluid interactions in mixed-wet shale pores. Fuel 319, 123587. https://doi.org/10.1016/i.fuel.2022.123587.
- Kirkwood, J.G., Boggs, E.M., 1942. The radial distribution function in liquids. J. Chem.

- Phys. 10 (6), 394-402. https://doi.org/10.1063/1.1723737.
- Kubo, R., 1957. Statistical-mechanical theory of irreversible processes. I. General theory and simple applications to magnetic and conduction problems. J. Phys. Soc. Jpn. 12 (6), 570–586. https://doi.org/10.1143/JPSI.12.570.
- Lan, Y., Yang, Z., Wang, P., et al., 2019. A review of microscopic seepage mechanism for shale gas extracted by supercritical CO₂ flooding. Fuel 238, 412–424. https:// doi.org/10.1016/j.fuel.2018.10.130.
- Lashgari, H.R., Sun, A., Zhang, T.W., et al., 2019. Evaluation of carbon dioxide storage and miscible gas EOR in shale oil reservoirs. Fuel 241, 1223–1235. https:// doi.org/10.1016/j.fuel.2018.11.076.
- Lee, S.H., Rossky, P.J., 1994. A comparison of the structure and dynamics of liquid water at hydrophobic and hydrophilic surfaces—a molecular dynamics simulation study. J. Chem. Phys. 100 (4), 3334–3345. https://doi.org/10.1063/ 1466425.
- Li, J.B., Jiang, C.Q., Wang, M., et al., 2020b. Adsorbed and free hydrocarbons in unconventional shale reservoir: a new insight from NMR T_1 - T_2 maps. Mar. Petrol. Geol. 116, 104311. https://doi.org/10.1016/j.marpetgeo.2020.104311.
- Li, M.W., Chen, Z.H., Qian, M.H., et al., 2020a. What are in pyrolysis S1 peak and what are missed? Petroleum compositional characteristics revealed from programed pyrolysis and implications for shale oil mobility and resource potential. Int. J. Coal Geol. 217, 103321. https://doi.org/10.1016/j.coal.2019.103321.
- Li, M.Y., Zhu, R.K., Hu, S.Y., 2022b. Geological characteristics and resource potential of overseas terrestrial shale oil. Lithologic Reservoirs 34 (1), 163–174. https://doi.org/10.12108/yxyqc.20220117. In Chinese.
- Li, W.H., Zhang, M.S., Nan, Y.L., et al., 2020c. Molecular dynamics study on CO₂ storage in water-filled kerogen nanopores in shale reservoirs: effects of kerogen maturity and pore size. Langmuir 37 (1), 542–552. https://doi.org/10.1021/acs.langmuir.0c03232.
- Li, X.F., Wang, S., Feng, Q.H., et al., 2020d. The miscible behaviors of $C_{10}H_{22}$ ($C_7H_{17}N$)/ C_3H_8 system: insights from molecular dynamics simulations. Fuel 279, 118445. https://doi.org/10.1016/j.fuel.2020.118445.
- Li, Y., Xu, J., Li, D., 2010. Molecular dynamics simulation of nanoscale liquid flows. Microfluid. Nanofluidics 9, 1011–1031. https://doi.org/10.1007/s10404-010-0612-5.
- Li, Y., Zhao, Q.M., Lyu, Q., et al., 2022a. Evaluation technology and practice of continental shale oil development in China. Petrol. Explor. Dev. 49 (5), 1098–1109. https://doi.org/10.1016/S1876-3804(22)60335-5.
- Li, Z., Wang, X.G., Kou, J.L., et al., 2024. Flow regime transition of multicomponent oil in shale nanopores. Fuel 359, 130431. https://doi.org/10.1016/j.fuel.2023.130431.
- Liang, S., Wang, J.M., Liu, Y.K., et al., 2022. Oil occurrence states in shale mixed inorganic matter nanopores. Front. Earth Sci. 9, 833302. https://doi.org/ 10.3389/feart.2021.833302.
- Liu, B., Liu, W.Y., Pan, Z.M., et al., 2022b. Supercritical CO₂ breaking through a water bridge and enhancing shale oil recovery: a molecular dynamics simulation study. Energy Fuels 36 (14), 7558–7568. https://doi.org/10.1021/acs.energyfuels.2c01547.
- Liu, B., Wang, C., Zhang, J., et al., 2017. Displacement mechanism of oil in shale inorganic nanopores by supercritical carbon dioxide from molecular dynamics simulations. Energy Fuels 31 (1), 738–746. https://doi.org/10.1021/ acs.energyfuels.6b02377.
- Liu, F., Gao, X., Du, J., et al., 2024. Microscopic mechanism of enhancing shale oil recovery through CO₂ flooding-insights from molecular dynamics simulations. J. Mol. Liq. 125593. https://doi.org/10.1016/j.molliq.2024.125593.
- Liu, J., Yang, Y.F., Sun, S.Y., et al., 2022a. Flow behaviors of shale oil in kerogen slit by molecular dynamics simulation. Chem. Eng. J. 434, 134682. https://doi.org/ 10.1016/j.cej.2022.134682.
- Liu, P., Harder, E., Berne, B.J., 2004. On the calculation of diffusion coefficients in confined fluids and interfaces with an application to the liquid –vapor interface of water. J. Phys. Chem. B 108 (21), 6595–6602. https://doi.org/10.1021/ jp0375057.
- Liu, P.C., Zhang, X.K., 2015. Enhanced oil recovery by CO₂-CH₄ flooding in low permeability and rhythmic hydrocarbon reservoir. Int. J. Hydrogen Energy 40 (37), 12849–12853. https://doi.org/10.1016/j.ijhydene.2015.07.013.
- Luan, Y.L., Liu, B., Hao, P., et al., 2020. Oil displacement by supercritical CO₂ in a water cut dead-end pore: molecular dynamics simulation. J. Petrol. Sci. Eng. 188, 106899. https://doi.org/10.1016/j.petrol.2019.106899.
- Luo, Y.C., Liu, X.G., Xiao, H.M., et al., 2023b. Microscopic production characteristics of tight oil in the nanopores of different CO₂-affected areas from molecular dynamics simulations. Separ. Purif. Technol. 306, 122607. https://doi.org/ 10.1016/j.seppur.2022.122607.
- Luo, Y.C., Xiao, H.M., Liu, X.G., et al., 2023a. Multiphase nanoconfined fluid flow mechanisms in nanopores, insights derived from molecular dynamics. Chem. Eng. J. 474, 145946. https://doi.org/10.1016/j.cej.2023.145946.
- Macintyre, K.J., 1986. Design considerations for carbon dioxide injection facilities. J. Can. Petrol. Technol. 25 (2). https://doi.org/10.2118/86-02-09.
- Makimura, D., Kunieda, M., Liang, Y., et al., 2013. Application of molecular simulations to CO₂-enhanced oil recovery: phase equilibria and interfacial phenomena. SPE J. 18 (2), 319–330. https://doi.org/10.2118/163099-PA.
- Mao, Q., Feng, M.Y., Jiang, X.Z., et al., 2023. Classical and reactive molecular dynamics: principles and applications in combustion and energy systems. Prog. Energy Combust. Sci. 97, 101084. https://doi.org/10.1016/j.pecs.2023.101084.
- Martin, M.G., Siepmann, J.I., 1998. Transferable potentials for phase equilibria. 1. United-atom description of n-alkanes. J. Phys. Chem. B 102 (14), 2569–2577. https://doi.org/10.1021/jp972543+.
- Marx, D., Hutter, J., 2009. Ab Initio Molecular Dynamics: Basic Theory and Advanced

Methods. Cambridge University Press. https://doi.org/10.1063/1.3366243.

- Mavroyannis, C., Stephen, M.J., 1962. Dispersion forces. Mol. Phys. 5 (6), 629–638.
 Mayo, S.L., Olafson, B.D., Goddard, W.A., 1990. DREIDING: A generic force field for molecular simulations. J. Phys. Chem. 94 (26), 8897–8909. https://doi.org/10.1021/j100389a010.
- McArdle, S., Endo, S., Aspuru-Guzik, A., et al., 2020. Quantum computational chemistry. Rev. Mod. Phys. 92 (1), 015003. https://doi.org/10.1103/RevModPhys.92.015003.
- Mercier Franco, L.F., Castier, M., Economou, I.G., 2016. Diffusion in homogeneous and in inhomogeneous media: A new unified approach. J. Chem. Theor. Comput. 12 (11), 5247–5255. https://doi.org/10.1021/acs.ictc.6b00653.
- Moh, D.Y., Zhang, H.W., Wang, S.H., et al., 2022. Soaking in CO₂ huff-n-puff: A single-nanopore scale study. Fuel 308, 122026. https://doi.org/10.1016/i.fuel.2021.122026.
- Mohammed, S., Mansoori, G.A., 2018. Molecular insights on the interfacial and transport properties of supercritical CO₂/brine/crude oil ternary system. J. Mol. Liq. 263, 268–273. https://doi.org/10.1016/j.molliq.2018.05.009. Moradi, M., Azizpour, H., Mohammarehnezhad-Rabieh, M., 2023. Determination of
- Moradi, M., Azizpour, H., Mohammarehnezhad-Rabieh, M., 2023. Determination of diffusion coefficient of C₂H₆ and CO₂ in hydrocarbon solvents by molecular dynamics simulation. J. Mol. Liq. 370, 121015. https://doi.org/10.1016/j.molliq.2022.121015.
- Obliger, A., Pellenq, R., Ulm, F.J., et al., 2016. Free volume theory of hydrocarbon mixture transport in nanoporous materials. J. Phys. Chem. Lett. 7 (19), 3712–3717. https://doi.org/10.1021/acs.jpclett.6b01684.
- Pang, X.Q., Li, M., Li, B.Y., et al., 2023. Main controlling factors and movability evaluation of continental shale oil. Earth-Sci. Rev. 104472. https://doi.org/10. 1016/j.earscirev.2023.104472.
- Payal, R.S., Balasubramanian, S., Rudra, I., Tandon, K., Mahlke, I., Doyle, D., Cracknell, R., 2012. Shear viscosity of linear alkanes through molecular simulations: quantitative tests for *n*-decane and *n*-hexadecane. Mol. Simulat. 38 (14–15), 1234–1241. https://doi.org/10.1080/08927022.2012.702423.
- Rahnamoun, A., Kaymak, M.C., Manathunga, M., Götz, A.W., Van Duin, A.C., Merz Jr, K.M., Aktulga, H.M., 2020. ReaxFF/AMBER—a framework for hybrid reactive/nonreactive force field molecular dynamics simulations. J. Chem. Theor. Comput. 16 (12), 7645–7654. https://doi.org/10.1021/acs.jctc.0c00874.
- Rapaport, D.C., 2004. The art of molecular dynamics simulation. Cambridge University Press. https://doi.org/10.1109/5992.743625.
- Rigby, D., Roe, R.J., 1988. Molecular dynamics simulation of polymer liquid and glass. II. Short range order and orientation correlation. J. Chem. Phys. 89 (8), 5280–5290. https://doi.org/10.1063/1.455619.
- Sambo, C., Liu, N., Shaibu, R., et al., 2023. A technical review of CO₂ for enhanced oil recovery in unconventional oil reservoirs. Geoenergy Science and Engineering 221, 111185. https://doi.org/10.1016/j.petrol.2022.111185.
- Sang, Q., Zhao, X.Y., Liu, H.M., et al., 2022. Analysis of imbibition of n-alkanes in kerogen slits by molecular dynamics simulation for characterization of shale oil rocks. Petrol. Sci. 19 (3), 1236–1249. https://doi.org/10.1016/ j.petsci.2022.01.005.
- Sedghi, M., Piri, M., Goual, L., 2016. Atomistic molecular dynamics simulations of crude oil/brine displacement in calcite mesopores. Langmuir 32 (14), 3375–3384. https://doi.org/10.1021/acs.langmuir.5b04713.
- Sheng, J.J., 2015. Enhanced oil recovery in shale reservoirs by gas injection. J. Nat. Gas Sci. Eng. 22, 252–259. https://doi.org/10.1016/j.jngse.2014.12.002.
- Si, J., Zhao, Z., Li, L., Cheng, G., et al., 2024. Optimization of CO₂/N₂ injection ratios in goaf by saturation adsorption capacity. Arab. J. Chem. 17 (6), 105804. https:// doi.org/10.1016/j.arabjc.2024.105804.
- Skoulidas, A.I., Ackerman, D.M., Johnson, J.K., et al., 2002. Rapid transport of gases in carbon nanotubes. Phys. Rev. Lett. 89 (18), 185901. https://doi.org/10.1103/PhysRevLett.89.185901.
- Song, Y.L., Song, Z.J., Guo, J., et al., 2020. Confinement effect on the fluid phase behavior and flow in shale oil reservoirs. In: SPE/AAPG/SEG Unconventional Resources Technology Conference. https://doi.org/10.15530/urtec-2020-3135.
- Sponer, J., Hobza, P., Leszczynski, J., 1999. Computational approaches to the studies of the interactions of nucleic acid bases. Theoretical and Computational Chemistry Vol. 8, 85–117. https://doi.org/10.1016/S1380-7323(99)80078-8.
- Sui, H.G., Zhang, F.Y., Wang, Z.Q., et al., 2020. Molecular simulations of oil adsorption and transport behavior in inorganic shale. J. Mol. Liq. 305, 112745. https:// doi.org/10.1016/j.molliq.2020.112745.
- Sui, H.G., Zhang, F.Y., Zhang, L., et al., 2023. Mechanism of CO₂ enhanced oil recovery in kerogen pores and CO₂ sequestration in shale: a molecular dynamics simulation study. Fuel 349, 128692. https://doi.org/10.1016/j.fuel.2023.128692.
- Sun, H., 1995. Ab initio calculations and force field development for computer simulation of polysilanes. Macromolecules 28 (3), 701–712. https://doi.org/ 10.1021/ma00107a006.
- Sun, H., Li, T.H., Li, Z., et al., 2023c. Shale oil redistribution-induced flow regime transition in nanopores. Energy 128553. https://doi.org/10.1016/j.energy.2023.128553.
- Sun, H., Ren, P., Fried, J.R., 1998. The COMPASS force field: parameterization and validation for phosphazenes. Comput. Theor. Polym. Sci. 8 (1–2), 229–246. https://doi.org/10.1016/S1089-3156(98)00042-7.
- Sun, Q., Bhusal, A., Zhang, N., et al., 2023b. Molecular insight into minimum miscibility pressure estimation of shale oil/CO₂ in organic nanopores using CO₂ huff-n-puff. Chem. Eng. Sci. 119024. https://doi.org/10.1016/j.ces.2023.119024.
- Sun, S., Liang, S., Liu, Y.K., et al., 2023a. A review on shale oil and gas characteristics and molecular dynamics simulation for the fluid behavior in shale pore. J. Mol. Liq. 121507. https://doi.org/10.1016/j.molliq.2023.121507.

Sun, Z., Li, X.F., Liu, W.Y., et al., 2020. Molecular dynamics of methane flow behavior through realistic organic nanopores under geologic shale condition: pore size and kerogen types. Chem. Eng. J. 398, 124341. https://doi.org/10.1016/ i.cei.2020.124341.

- Takbiri-Borujeni, A., Kazemi, M., Liu, S.Y., et al., 2019. Molecular simulation of enhanced oil recovery in shale. Energy Proc. 158, 6067–6072. https://doi.org/ 10.1016/j.egypro.2019.01.510.
- Teklu, T.W., Alharthy, N., Kazemi, H., et al., 2014. Phase behavior and minimum miscibility pressure in nanopores. SPE Reservoir Eval. Eng. 17 (3), 396–403. https://doi.org/10.2118/168865-PA.
- Tian, S.S., Xue, H.T., Lu, S.F., et al., 2017. Molecular simulation of oil mixture adsorption character in shale system. J. Nanosci. Nanotechnol. 17 (9), 6198–6209. https://doi.org/10.1166/jnn.2017.14487.
- Tian, S.S., Erastova, V., Lu, S.F., et al., 2018. Understanding model crude oil component interactions on kaolinite silicate and aluminol surfaces: toward improved understanding of shale oil recovery. Energy Fuels 32 (2), 1155–1165. https://doi.org/10.1021/acs.energyfuels.7b02763.
- Tinni, A., Sondergeld, C.H., Rai, C.S., 2017. Hydrocarbon storage mechanism in shale reservoirs and impact on hydrocarbon production. In: Unconventional Resources Technology Conference. https://doi.org/10.15530/urtec-2017-2697659.
- U.S. Energy Information Administration, 2022. Assumptions to the annual energy outlook 2022: oil and gas supply module. Washington, DC, United States: analysis & projections, 2022. https://www.eia.gov/outlooks/aeo/assumptions/ pdf/oilgas.
- Underwood, T., Erastova, V., Cubillas, P., et al., 2015. Molecular dynamic simulations of montmorillonite—organic interactions under varying salinity: an insight into enhanced oil recovery. J. Phys. Chem. C 119 (13), 7282–7294. https://doi.org/ 10.1021/acs.jpcc.5b00555.
- Van Buuren, A.R., Marrink, S.J., Berendsen, H.J., 1993. A molecular dynamics study of the decane/water interface. J. Phys. Chem. 97 (36), 9206–9212. https://doi.org/ 10.1021/j100138a023.
- Van Gunsteren, W.F., Berendsen, H.J., 1990. Computer simulation of molecular dynamics: methodology, applications, and perspectives in chemistry. Angew Chem. Int. Ed. Engl. 29 (9), 992–1023. https://doi.org/10.1002/anie.199009921.
- Vanommeslaeghe, K., MacKerell Jr, A.D., 2012. Automation of the CHARMM general force field (CGenFF) I: bond perception and atom typing. J. Chem. Inf. Model. 52 (12), 3144–3154. https://doi.org/10.1021/ci300363c.
- Vanommeslaeghe, K., Raman, E.P., MacKerell Jr, A.D., 2012. Automation of the CHARMM General Force Field (CGenFF) II: assignment of bonded parameters and partial atomic charges. J. Chem. Inf. Model. 52 (12), 3155–3168. https://doi.org/10.1021/ci3003649.
- Vinogradova, O.I., Yakubov, G.E., 2006. Surface roughness and hydrodynamic boundary conditions. Phys. Rev. 73 (4), 045302. https://doi.org/10.1103/PhysRevE.73.045302.
- Von Smoluchowski, M., 1906. Zur kinetischen theorie der brownschen molekularbewegung und der suspensionen. Ann. Phys. 326 (14), 756–780. https://doi.org/10.1002/andp.19063261405.
- Wang, H., Qu, Z., Yin, Y., et al., 2019. Review of molecular simulation method for gas adsorption/desorption and diffusion in shale matrix. J. Therm. Sci. 28, 1–16. https://doi.org/10.1007/s11630-018-1053-9.
- Wang, L., Lyu, W.F., Ji, Z.M., et al., 2022b. Molecular dynamics insight into the CO₂ Flooding mechanism in wedge-shaped pores. Molecules 28 (1), 188. https://doi.org/10.3390/molecules28010188.
- Wang, L., Zhang, Y.F., Liu, Y.S., et al., 2023b. Molecular dynamics analysis on occurrence characteristics of shale oil and competitive adsorption mechanism of CO₂ and oil. Journal of China University of Petroleum (Edition of Natural Science) 47 (4), 128–136. https://doi.org/10.3969/j.issn.1673-5005.2023.04.013
- Wang, L., Zhang, Y.F., Zou, R., et al., 2023a. A systematic review of CO₂ injection for enhanced oil recovery and carbon storage in shale reservoirs. Int. J. Hydrogen Energy. https://doi.org/10.1016/j.ijhydene.2023.06.099.
- Wang, L., Zhang, Y.F., Zou, R., et al., 2023c. Molecular dynamics investigation of DME assisted CO₂ injection to enhance shale oil recovery in inorganic nanopores. J. Mol. Liq. 122389. https://doi.org/10.1016/j.molliq.2023.122389.
- Wang, S., Feng, Q.H., Javadpour, F., et al., 2015. Oil adsorption in shale nanopores and its effect on recoverable oil-in-place. Int. J. Coal Geol. 147, 9–24. https://doi.org/ 10.1016/j.coal.2015.06.002.
- Wang, S., Javadpour, F., Feng, Q.H., 2016a. Fast mass transport of oil and supercritical carbon dioxide through organic nanopores in shale. Fuel 181, 741–758. https:// doi.org/10.1016/j.fuel.2016.05.057.
- Wang, S., Javadpour, F., Feng, Q.H., 2016b. Molecular dynamics simulations of oil transport through inorganic nanopores in shale. Fuel 171, 74–86. https:// doi.org/10.1016/j.fuel.2015.12.071.
- Wang, S., Liang, Y.P., Feng, Q.H., et al., 2022a. Sticky layers affect oil transport through the nanopores of realistic shale kerogen. Fuel 310, 122480. https:// doi.org/10.1016/j.fuel.2021.122480.
- Wang, S., Wang, J., Zhang, H.Q., et al., 2023d. Layered threshold pressure of tight oil in nanopores: a Molecular dynamics simulation study. Energy Fuels 37 (14), 10235–10247. https://doi.org/10.1021/acs.energyfuels.3c01255.
- Wang, T., Tian, S., Li, G., et al., 2021. Molecular simulation of gas adsorption in shale nanopores: a critical review. Renew. Sustain. Energy Rev. 149, 111391. https:// doi.org/10.1016/j.rser.2021.111391.
- Wang, Y.Z., Cao, R.Y., Jia, Z., et al., 2024. A multi-mechanism numerical simulation model for CO₂-EOR and storage in fractured shale oil reservoirs. Petrol. Sci. 21 (3), 1814–1828. https://doi.org/10.1016/j.petsci.2024.02.006.

Wang, L., Zhang, Y.F., Zou, R., et al., 2025. Dynamics of oil–CO₂—water three-phase under the nanopore confinement effect: implications for CO₂ enhanced shale oil recovery and carbon storage. Separ. Purif. Technol. 354, 128892. https://doi.org/10.1016/j.seppur.2024.128892.

- Wang, Z.J., Zhu, J.Z., Li, S.Y., 2023e. Novel strategy for reducing the minimum miscible pressure in a CO₂—oil system using nonionic surfactant: insights from molecular dynamics simulations. Appl. Energy 352, 121966. https://doi.org/10.1016/j.apenergy.2023.121966.
- Wu, T.T., Xue, Q.Z., Li, X.F., et al., 2016. Extraction of kerogen from oil shale with supercritical carbon dioxide: molecular dynamics simulations. J. Supercrit. Fluids 107, 499–506. https://doi.org/10.1016/j.supflu.2015.07.005.
- Xiong, C.M., Li, S.J., Ding, B., et al., 2021. Molecular insight into the oil displacement mechanism of gas flooding in deep oil reservoir. Chem. Phys. Lett. 783, 139044. https://doi.org/10.1016/j.cplett.2021.139044.
- Xiong, H., Devegowda, D., 2022. Fluid behavior in clay-hosted nanopores with varying salinity: insights into molecular dynamics. SPE J. 27 (3), 1396–1410. https://doi.org/10.2118/209212-PA
- Xiong, H., Devegowda, D., Huang, L.L., 2020. Water bridges in clay nanopores: mechanisms of formation and impact on hydrocarbon transport. Langmuir 36 (3), 723–733. https://doi.org/10.1021/acs.langmuir.9b03244.
- Xu, J.L., Zhan, S.Y., Wang, W.D., et al., 2022b. Molecular dynamics simulations of two-phase flow of n-alkanes with water in quartz nanopores. Chem. Eng. J. 430, 132800. https://doi.org/10.1016/j.cej.2021.132800.
- Xu, Y., Lun, Z.M., Pan, Z.J., et al., 2022a. Occurrence space and state of shale oil: a review. J. Petrol. Sci. Eng. 211, 110183. https://doi.org/10.1016/ j.petrol.2022.110183.
- Xue, C.L., Ji, D.L., Cheng, D., et al., 2022. Adsorption behaviors of different components of shale oil in quartz slits studied by molecular simulation. ACS Omega 7 (45), 41189–41200. https://doi.org/10.1021/acsomega.2c04845.
- Xue, Q.Z., Tao, Y.H., Liu, Z.L., et al., 2015. Mechanism of oil molecules transportation in nano-sized shale channel: MD simulation. RSC Adv. 5 (33), 25684–25692. https://doi.org/10.1039/C4RA16682F.
- Yang, Y.F., Song, H.S., Imani, G., et al., 2023. Adsorption behavior of shale oil and water in the kerogen-kaolinite pore by molecular simulations. J. Mol. Liq. 123549. https://doi.org/10.1016/j.molliq.2023.123549.
- Yu, T., Li, Q., Tan, Y.S., et al., 2022. Molecular dynamics simulation of CO₂-N₂ dissolution and stripping of oil films on pore walls based on intermolecular interaction energy. Chem. Eng. Sci. 262, 118044. https://doi.org/10.1016/j.ces.2022.118044.
- Yu, Yang, Sheng, J.J., 2017. A comparative experimental study of IOR potential in fractured shale reservoirs by cyclic water and nitrogen gas injection. J. Petrol. Sci. Eng. 149, 844–850. https://doi.org/10.1016/j.petrol.2016.11.034.
- Yuan, L., Zhang, Y., Liu, S.Z., et al., 2023. Molecular dynamics simulation of CO₂-oil miscible fluid distribution and flow within nanopores. J. Mol. Liq. 380, 121769. https://doi.org/10.1016/j.molliq.2023.121769.
- Zeng, P.H., Ye, Z.B., Zhang, X.C., et al., 2023. Molecular dynamics simulation of shale oil adsorption on quartz surface with different wettability. J. At. Mol. Phys. 40, 036005. https://doi.org/10.19855/j.1000-0364.2023.036005 (in Chinese).
- Zhan, S.Y., Su, Y.L., Jin, Z.H., et al., 2020. Effect of water film on oil flow in quartz nanopores from molecular perspectives. Fuel 262, 116560. https://doi.org/10.1016/j.fuel.2019.116560.
- Zhang, B., Kang, J.T., Kang, T.H., 2018b. Molecular simulation of methane adsorption and its effect on kaolinite swelling as functions of pressure and temperature. Mol. Simulat. 44 (10), 789–796. https://doi.org/10.1080/ 08927022.2018.1453138.
- Zhang, H.Y., Ahmed, M., Zhan, J.H., 2022. Recent advances in molecular simulation of oil shale kerogen. Fuel 316, 123392. https://doi.org/10.1016/j.fuel.2022.123392.
- Zhang, L.H., Lu, X.C., Liu, X.D., et al., 2016. Surface wettability of basal surfaces of clay minerals: insights from molecular dynamics simulation. Energy Fuels 30 (1), 149–160. https://doi.org/10.1021/acs.energyfuels.5b02142.
- Zhang, L.H., Lu, X.C., Liu, X.D., et al., 2019a. Distribution and mobility of crude oil—brine in clay mesopores: insights from molecular dynamics simulations. Langmuir 35 (46), 14818—14832. https://doi.org/10.1021/acs.langmuir.9b02925.
- Zhang, W., Feng, Q.H., Wang, S., et al., 2019b. Oil diffusion in shale nanopores: insight of molecular dynamics simulation. J. Mol. Liq. 290, 111183. https://doi.org/10.1016/j.molliq.2019.111183.
- Zhang, W., Feng, Q.H., Wang, S., et al., 2021. Molecular simulation of water effect on oil transport in montmorillonite nanopore of shale. In: Proceedings of the International Field Exploration and Development Conference 2020, pp. 2408–2417. https://doi.org/10.1007/978-981-16-0761-5_227.
- Zhang, Y., Yu, W., Li, Z.P., et al., 2018a. Simulation study of factors affecting CO₂ Huff-n-Puff process in tight oil reservoirs. J. Petrol. Sci. Eng. 163, 264–269. https://doi.org/10.1016/j.petrol.2017.12.075.
- Zhang, Y.F., Wang, L., Zou, R., et al., 2023a. Effect of cosolvents on CO₂ replacement of shale oil and carbon storage. Petrol. Explor. Dev. 50 (6), 1318–1326. https://doi.org/10.11698/PED.20230261.
- Zhang, Y.N., Li, S.J., Dou, X.J., et al., 2023b. Molecular insights into the natural gas regulating tight oil movability. Energy 270, 126895. https://doi.org/10.1016/ j.energy.2023.126895.
- Zhang, Z.L., Liu, H.R., Wang, J.W., 2020. Energetics of interfacial interactions of hydrocarbon fluids with kerogen and calcite using molecular modeling. Energy Fuels 34 (4), 4251–4259. https://doi.org/10.1021/acs.energyfuels.0c00053.
- Zhao, J., Yao, G.C., Ramisetti, S.B., et al., 2019. Molecular dynamics investigation of substrate wettability alteration and oil transport in a calcite nanopore. Fuel 239,

- 1149-1161. https://doi.org/10.1016/j.fuel.2018.11.089.
- Zhao, X.Y., Sang, Q., Li, Y.J., et al., 2021a. CO₂-kerogen interaction dominated CO₂-oil counter-current diffusion and its effect on ad-/absorbed oil recovery and CO₂ sequestration in shale. Fuel 294, 120500. https://doi.org/10.1016/j.fuel.2021.120500.
- Zhao, X.Y., Sang, Q., Li, Y.J., et al., 2021b. Mobilization of oil in organic matter and its contribution to oil production during primary production in shale. Fuel 287, 119449. https://doi.org/10.1016/j.fuel.2020.119449.
- Zhou, L.H., Chen, C.W., Yang, F., et al., 2020. Micropore structure characteristics and
- quantitative characterization methods of lacustrine shale-A case study from the member 2 of Kongdian Formation, Cangdong sag, Bohai Bay Basin. Petroleum Research 5 (2), 93—102. https://doi.org/10.1016/j.ptlrs.2020.01.001.
 Zhu, C.F., Qin, X.J., Li, Y.J., et al., 2019. Adsorption and dissolution behaviors of CO₂
- Zhu, C.F., Qin, X.J., Li, Y.J., et al., 2019. Adsorption and dissolution behaviors of CO₂ and n-alkane mixtures in shale: Effects of the alkane type, shale properties and temperature. Fuel 253, 1361–1370. https://doi.org/10.1016/j.fuel.2019.05.002.
- Zhu, W.Y., Pan, B., Chen, Z., et al., 2023. Mining science, technology, and engineering—review transport in nanoporous media. Engineering 32, 138–151. https://doi.org/10.1016/j.eng.2023.05.014.